We are IntechOpen, the world's leading publisher of Open Access books Built by scientists, for scientists

6,900
Open access books available

185,000
International authors and editors

200M
Downloads

Our authors are among the

154
Countries delivered to

TOP 1%
most cited scientists

12.2%
Contributors from top 500 universities

WEB OF SCIENCE™

Selection of our books indexed in the Book Citation Index in Web of Science™ Core Collection (BKCI)

Interested in publishing with us?
Contact book.department@intechopen.com

Numbers displayed above are based on latest data collected.
For more information visit www.intechopen.com

4

A Mathematical Model for Single Crystal Cylindrical Tube Growth by the Edge-Defined Film-Fed Growth (EFG) Technique

Loredana Tanasie and Stefan Balint
West University of Timisoara
Romania

1. Introduction

1.1 Crystal growth from the melt by E.F.G. technique

Modern engineering does not only need crystals of arbitrary shapes but also plate, rod and tube-shaped crystals, i.e., crystals of shapes that allow their use as final products without additional machining. Therefore, the growth of crystals of specified sizes and shapes with controlled defect and impurity structures are required. In the case of crystals grown from the melt, this problem appears to be solved by profiled-container crystallization as in the case of casting. However, this solution is not always possible, for example growing very thin plate-shaped crystals from the melt (to say nothing of more complicated shapes), excludes container application completely.[Tatarchenko, 1993]

The techniques which allow the shaping of the lateral crystal surface without contact with the container walls are appropriate for the above purpose. In the case of these techniques the shapes and the dimensions of the grown crystals are controlled by the interface and meniscus-shaping capillary force and by the heat- and mass-exchange conditions in the crystal-melt system. The edge-defined film-fed growth (EFG) technique is of this type. Whenever the E.F.G. technique is employed, a shaping device is used (Fig. 1). In the device a capillary channel is manufactured (Fig. 1) in which the melt raises and feeds the growth process. Frequently, a wettable solid body is used to raise the melt column above the shaper, where a thin film is formed. When a wettable body is in contact with the melt, an equilibrium liquid column embracing the surface of the body is formed. The column formation is caused by the capillary forces being present. Such liquid configuration is usually called a meniscus (Fig. 1) and in the E.F.G. technique, its lower boundary (Fig. 1 – point C) is attached to the sharp edge of the shaper.

Let be the temperature of the meniscus upper horizontal section (Fig. 1 – $\overline{AB}$) the temperature of the liquid crystallization. So, above the plane of this section, the melt transforms in solid phase. Now set the liquid phase into upward motion with the constant rate, v, keeping the position of the phase-transition plane invariable by selection of the heat conditions. When the motion starts, the crystallized position of the meniscus will

continuously form a solid upward or downward tapering body. In the particular case when the line tangent at the triple point B to the liquid meniscus surface makes a specific angle (angle of growth) with the vertical, the lateral wall of the crystal will be vertical. Thus, the initial body, called the seed, serves to form a meniscus which later on determines the form of the crystallized product, the phase transition position being fixed.

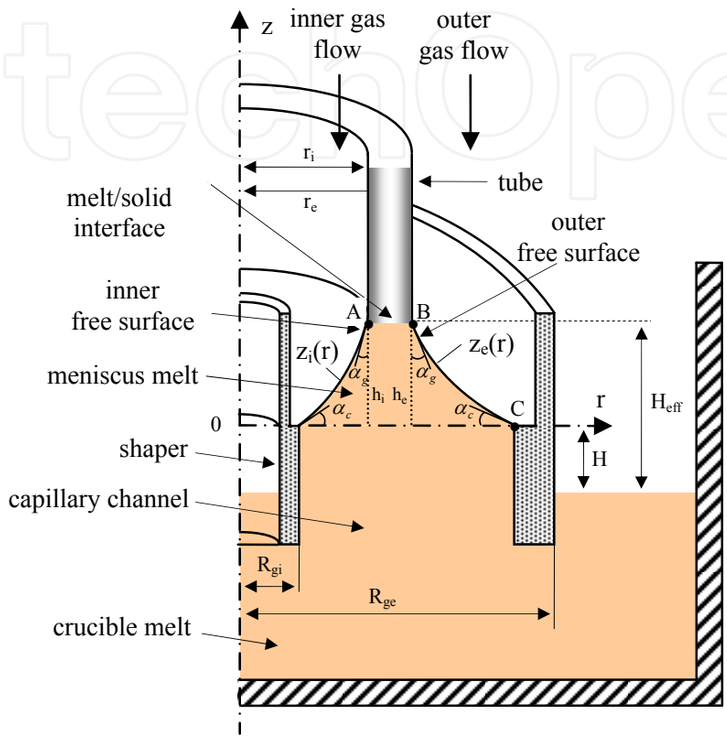

Fig. 1. Prototype tubular crystal growth by E.F.G. method

Based on this description, a conclusion can be drawn that the dimensions and shapes of the specimens being pulled by the E.F.G. technique depend upon the following factors: (i) the shaper geometry; (ii) the pressure of feeding the melt to the shaper; (iii) the crystallization front position; (iv) the seed's shape. The seed's shape is only important for stationary pulling; in this case its cross-section should coincide with the desired product's cross-section. Frequently, especially when complicated profiles are grown, the pulling process is carried out under unstationary conditions by lowering the crystallization surface, which then enhances the dependence of the shapes on the crystal cross-section. With such an approach applied to the pulling process, the dimensions and the shape of the grown crystal are determined by the above-mentioned factors and by the pulling rate-to-crystallization front displacement ratio.[Tatarchenko, 1993].

1.2 Background history of tube growth from the melt by E.F.G. method

The technology of growing tubes can have a significant impact for example on the solar cell technology. The growth of silicon tubes by E.F.G. process was first reported by Erris et al. [Erris et al.,1980]. Tubes were grown with a diameter of 95×10^{-4} [m], wall thickness in the

range of $5\times10^{-5}-1\times10^{-3}$ [m] at rates up to 2×10^{-3} [m/s]. In [Erris et al.,1980] a theory of tube growth by the E.F.G. process is developed to show the dependence of the tube wall thickness on the growth variables. The theory concerns the calculations of the shape of the liquid-vapor interface (or meniscus) and of the heat flow in the system. The inner and outer meniscus shapes, (Fig.1), are both calculated from Laplace's capillary equation, in which the pressure difference Δp across a point on meniscus is considered to be $\Delta p = \rho \circledcirc g \circledcirc H_{eff}$ = constant, where H_{eff} represents the effective height of the growth interface above the horizontal liquid level in the crucible (Fig.1). According to [Surek et al.,1977], [Swartz et al., 1975], it includes the effects of the viscous flow of the melt in the shaper capillary and in the meniscus film, as well as that of the hydrostatic head. The above approximation for Δp is valid for silicon ribbon growth [Surek et al.,1977], [Kalejs et al., 1990], when $H_{eff} >> h$, where h is the height of the growth interface above the shaper top (i.e. the meniscus height). Another approximation used in [Erris et al.,1980], concerning the meniscus, is that the inner and outer meniscus shapes are approximated by circular segments. With these relatively tight tolerances concerning the menisci in conjunction with the heat flow calculation in the system, the predictive model developed in [Erris et al.,1980] has been shown to be a useful tool in understanding the feasible limits of wall thickness control. A more precise predictive model would require an increase of the acceptable tolerance range introduced by approximation.

Later, this process was scaled up by Kaljes et al. [Kalejs et al., 1990] to grow 15×10^{-2} [m] diameter silicon tubes, and the stress behavior in the grown tube was investigated. It has been realized that numerical investigations are necessary for the improvement of the technology. Since the growth system consists of a small die tip (1×10^{-3} m width) and a thin tube (order of 200×10^{-6} [m] wall thickness) the width of the melt/solid interface and meniscus are accordingly very small. Therefore, it is essential to obtain an accurate solution for the temperature and interface position in this tiny region.

In [Rajendran et al., 1993] an axisymmetric finite element model of magnetic and thermal field was presented for an inductively heated furnace. Later the same model was used to determine the critical parameters controlling silicon carbide precipitation on the die wall [Rajendran et al., 1994]. Rajendran et al. also developed a three dimensional magnetic induction model for an octagonal E.F.G, system. Recently, in [Roy et al., 2000a], [Roy et al., 2000b], a generic numerical model for an inductively heated large diameter Si tube growth system was reported. In [Sun et al., 2004] a numerical model based on multi-block method and multi-grid technique is developed for induction heating and thermal transport in an E.F.G. system. The model is applied to investigate the growth of large octagon silicon tubes of up to 50×10^{-2} m diameter. A 3D dynamic stress model for the growth of hollow silicon polygons is reported in [Behnken et al., 2005]. In [Mackintosh et al., 2006] the challenges fixed in bringing E.F.G. technology into large-scale manufacturing, and ongoing development of furnace designs for growth of tubes for larger wafer production using hexagons with 1×10^{-2} m face widths, and wall thicknesses in he range $250\times10^{-6}-300\times10^{-6}$ m is described. In [Kasjanow et al., 2010] the authors present a 3D coupled electromagnetic and thermal modeling of E.F.G. silicon tube growth, successfully validated by experimental tests with industrial installations.

The state of the art at 1993-1994 concerning the calculation of the meniscus shape in general in the case of the growth by E.F.G. method is summarized in [Tatarchenko, 1993]. According to [Tatarchenko, 1993], for the general equation describing the surface of a liquid meniscus possessing axial symmetry, there is no complete analysis and solution. For the general equation only numerical integration was carried out for a number of process parameter values that are of practical interest at the moment. The authors of papers [Borodin&Borodin&Sidorov&Petkov, 1999],[Borodin&Borodin&Zhdanov, 1999] consider automated crystal growth processes based on weight sensors and computers. They give an expression for the weight of the meniscus, contacted with a crystal and shaper of arbitrary shape, in which there are two terms related to the hydrodynamic factor. In [Rosolenko et al., 2001] it is shown that the hydrodynamic factor is too small to be considered in the automated crystal growth and it is not clear what equation (of non Laplace type) was considered for the meniscus surface. Finally, in [Yang et al., 2006] the authors present theoretical and numerical study of meniscus dynamics under symmetric and asymmetric configurations. A meniscus dynamics model is developed to consider meniscus shape and its dynamics, heat and mass transfer around the die-top and meniscus. Analysis reveals the correlations between tube thickness, effective melt height, pull-rate, die-top temperature and crystal environmental temperature.

The purpose of this chapter is the mathematical description of the growth process of a single crystal cylindrical tube grown by the edge-defined film-fed growth (EFG) technique. The mathematical model defined by a set of three differential equations governing the evolution of the outer radius and the inner radius of the tube and of the crystallization front level is the one considered in [Tatarchenko, 1993]. This system contains two functions which represent the angle made by the tangent line to the outer (inner) meniscus surface at the three-phase point with the horizontal. The meniscus surface is described mathematically by the solution of the axi-symmetric Young-Laplace differential equation. The analysis of the dependence of solutions of the Young-Laplace differential equation on the pressure difference across the free surface, reveals necessary or sufficient conditions for the existence of solutions which represent convex or concave outer or inner free surfaces of a meniscus. These conditions are expressed in terms of inequalities which are used for the choice of the pressure difference, in order to obtain a single-crystal cylindrical tube with specified sizes.

A numerical procedure for determining the functions appearing in the system of differential equations governing the evolution is presented.

Finally, a procedure is presented for setting the pulling rate, capillary and thermal conditions to grow a cylindrical tube with prior established inner and outer radius. The right hand terms of the system of differential equations serve as tools for setting the above parameters. At the end a numerical simulation of the growth process is presented.

The results presented in this chapter were obtained by the authors and have never been included in a book concerning this topic.

Since the calculus and simulation in this model can be made by a P.C., the information obtained in this way is less expressive than an experiment and can be useful for experiment planing.

2. The system of differential equations which governs the evolution of the tube's inner radius r_i, outer radius r_e and the level of the crystallization front h

According to [Tatarchenko, 1993] the system of differential equations which governs the evolution of the tube's inner radius r_i, the outer radius r_e and the level of the crystallization front h is:

$$\begin{cases} \dfrac{dr_e}{dt} = -v \cdot \tan\left[\bar{\alpha}_e(r_e,h,p_e) - \left(\dfrac{\pi}{2} - \alpha_g\right)\right] \\ \dfrac{dr_i}{dt} = v \cdot \tan\left[\bar{\alpha}_i(r_i,h,p_i) - \left(\dfrac{\pi}{2} - \alpha_g\right)\right] \\ \dfrac{dh}{dt} = v - \dfrac{1}{\Lambda \cdot \rho_1} \cdot \left[\lambda_1 \cdot G_1(r_e,r_i,h) - \lambda_2 \cdot G_2(r_e,r_i,h)\right] \end{cases} \quad (1)$$

In equations $(1)_1$ and $(1)_2$: v is the pulling rate, $\bar{\alpha}_e(r_e,h,p_e)$ ($\bar{\alpha}_i(r_i,h,p_i)$) is the angle between the tangent line to the outer (inner) meniscus at the three phase point of coordinates (r_e,h) ((r_i,h)) and the horizontal Or axis (Fig.1 b), α_g is the growth angle (Fig. 1), p_e (p_i) is the controllable part of the pressure difference across the free surface given by:

$$p_e = p_m - p_g^e - \rho_1 \cdot g \cdot H_e \ (p_i = p_m - p_g^i - \rho_1 \cdot g \cdot H_i) \quad (2)$$

where p_m is the hydrodynamic pressure in the melt under the free surface, which can be neglected in general, with respect to the hydrostatic pressure $\rho_1 \cdot g \cdot H_e$ ($\rho_1 \cdot g \cdot H_i$); p_g^e (p_g^i) is the pressure of the gas flow, introduced in order to release the heat from the outer (inner) wall of the tube; H_e (H_i) is the melt column height between the horizontal crucible melt level and the shaper outer (inner) top level (Fig. 1a); ρ_1 is the melt density; g is the gravity acceleration.

The angle $\bar{\alpha}_e(r_e,h,p_e)$ ($\bar{\alpha}_i(r_i,h,p_i)$) fluctuates due to the fluctuations of: the outer (inner) radius r_e (r_i), the level h of the crystallization front and the outer (inner) pressure p_e (p_i)

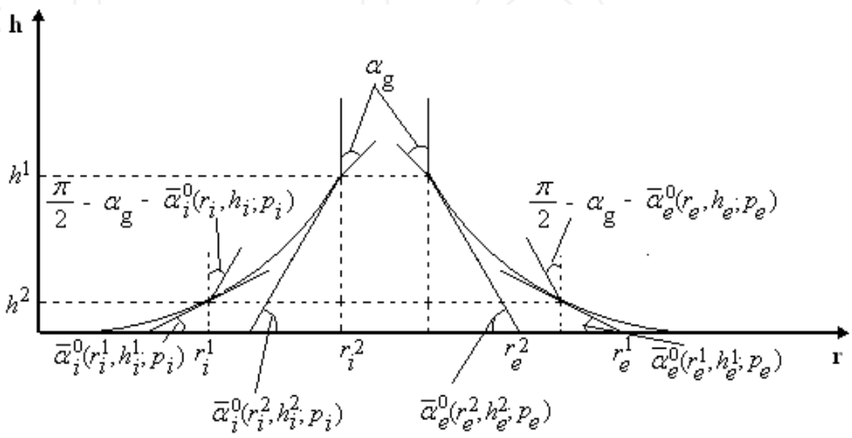

Fig. 2. Fluctuations at the triple point

In the equation $(1)_3$: Λ is the latent melting heat; λ_1, λ_2 are the thermal conductivity coefficients in the melt and the crystal respectively; G_1^j, G_2^j are the temperature gradients at the interface in the melt *(i=1)* and in the crystal *(i=2)* respectively, given by the formulas:

$$G_1^j(r_e, r_i, h) = \frac{1}{SINH(\beta_{1j} \cdot h)} \left[\left(T_0 - T_{en}(0) - \frac{v \cdot k}{(F_j)^2 \cdot Bi \cdot \chi_1} \right) \cdot \left(-\beta_{1j} \cdot e^{\delta_1 \cdot h} \right) + \left(T_m - T_{en}(0) + k \cdot h - \frac{v \cdot k}{(F_j)^2 \cdot Bi \cdot \chi_1} \right) \cdot \left(\delta_1 \cdot SINH(\beta_{1j} \cdot h) + \beta_{1j} \cdot COSH(\beta_{1j} \cdot h) \right) \right] - k \tag{3}$$

$$G_2^j(r_e, r_i, h) = \frac{1}{SINH(\beta_{2j} \cdot L)} \left[\left(T_m - T_{en}(0) + k \cdot h - \frac{v \cdot k}{(F_j)^2 \cdot Bi \cdot \chi_2} \right) \cdot \left(\delta_2 \cdot SINH(\beta_{2j} \cdot L) - \beta_{2j} \cdot COSH(\beta_{2j} \cdot L) \right) - \frac{v \cdot k}{(F_j)^2 \cdot Bi \cdot \chi_2} \cdot \beta_{2j} \cdot e^{-\delta_2 \cdot L} \right] - k \tag{4}$$

where χ_i - the thermal diffusivity coefficient equal to $\frac{\lambda_i}{\rho_i \cdot c_i}$, ρ_i - the density, c_i - the heat capacity, Bi - the Biot number equal to $\frac{\mu_i \cdot r_e}{\lambda_i}$ (*i=1* - the melt, *i=2* - the crystal), $\mu_i = \mu_i^k + \mu_i^r$ - the coefficient of the heat-exchange with environment (μ_i^k - the convective heat-exchange coefficient and μ_i^r - the linearized radiation heat-exchange coefficient), F_j ($j = 1,2,3$) the crystal (meniscus) cross – section perimeter – to – its area ratio: $j = 1$ and $F_1 = \frac{2}{r_e}$, for a thick-walled tube with small inner radius, for which heat is removed from the external surface only, $j = 2$ and $F_2 = \frac{2 \cdot r_e}{r_e^2 - r_i^2}$ for a tube of not to large inner radius for which heat is removed from the external surface only, $j = 3$ and $F_3 = \frac{2}{r_e - r_i}$ for a tube for which heat is removed from both the outer and inner surfaces([Tatarchenko, 1993], pp. 39-40, 146). T_0 - the melt temperature at the meniscus basis, T_m - melting temperature, $T_{en}(0)$ - the environment temperature at $z = 0$, k - the vertical temperature gradient in the furnace, r_e - the outer radius of the tube equal to the upper radius of the outer meniscus, r_i - the inner radius of the tube equal to the upper radius of the inner meniscus, L - the tube length and $\delta_i = \frac{v}{2\chi_i}$, $\beta_{ij} = \sqrt{\frac{v^2}{4\chi_i^2} + (F_j)^2 \cdot Bi}$, $i = 1,2$, $j = 1,2,3$, *SINH* and *COSH* are the hyperbolic sine and hyperbolic cosine functions.

Due to the supercooling in this gradients it is assumed that: $T_0 < T_m$, $k > 0$, $T_{en}(0) < T_m$.

In the following sections we will show in which way $\overline{\alpha}_e(r_e,h,p_e)$ and $\overline{\alpha}_i(r_i,h,p_i)$ can be found starting from the Young-Laplace equation of a capillary surface in equilibrium.

3. The choice of the pressure of the gas flow and the melt level in silicon tube growth

In a single crystal tube growth by edge-defined film-fed growth (E.F.G.) technique, in hydrostatic approximation, the free surface of a static meniscus is described by the Young-Laplace capillary equation [Finn, 1986]:

$$\gamma\cdot\left(\frac{1}{R_1}+\frac{1}{R_2}\right)=\rho\cdot g\cdot z-p \tag{5}$$

Here γ is the melt surface tension, ρ denotes the melt density, g is the gravity acceleration, $1/R_1, 1/R_2$ denote the mean normal curvatures of the free surface at a point M of the free surface, z is the coordinate of M with respect to the Oz axis, directed vertically upwards, p is the pressure difference across the free surface. To calculate the outer and inner free surface shape of the static meniscus it is convenient to employ the Young-Laplace eq.(5) in its differential form. This form of the eq.(5) can be obtained as a necessary condition for the minimum of the free energy of the melt column [Finn, 1986].For a tube of outer radius $r_e\in\left(\frac{R_{gi}+R_{ge}}{2},R_{ge}\right)$ and inner radius $r_i\in\left(R_{gi},\frac{R_{gi}+R_{ge}}{2}\right)$, the axi-symmetric differential equation of the outer free surface is given by:

$$z''=\frac{\rho\cdot g\cdot z-p_e}{\gamma}\left[1+(z')^2\right]^{3/2}-\frac{1}{r}\cdot\left[1+(z')^2\right]\cdot z' \quad \text{for} \quad r\in[r_e,R_{ge}] \tag{6}$$

which is the Euler equation for the energy functional

$$\begin{aligned} &I_e(z)=\int_{r_e}^{R_{ge}}\left\{\gamma\cdot\left[1+(z')^2\right]^{1/2}+\frac{1}{2}\cdot\rho\cdot g\cdot z^2-p_e\cdot z\right\}\cdot r\cdot dr,\quad z(r_e)=z_e(r_e),\\ &z(R_{ge})=z_e(R_{ge})=0 \end{aligned} \tag{7}$$

The axi-symmetric differential equation of the inner free surface is given by:

$$z''=\frac{\rho\cdot g\cdot z-p_i}{\gamma}\left[1+(z')^2\right]^{3/2}-\frac{1}{r}\cdot\left[1+(z')^2\right]\cdot z' \quad \text{for} \quad r\in\left[R_{gi},r_i\right] \tag{8}$$

which is the Euler equation for the energy functional:

$$I_i(z)=\int_{R_{gi}}^{r_i}\left\{\gamma\cdot\left[1+(z')^2\right]^{1/2}+\frac{1}{2}\cdot\rho\cdot g\cdot z^2-p\cdot z\right\}\cdot r\cdot dr,\quad z(R_{gi})=z_i(R_{gi})=0,\quad z(r_i)=z_i(r_i) \tag{9}$$

In papers [Balint & Balint, 2009b], [Balint&Balint&Tanasie, 2008], [Balint & Tanasie, 2008] , Balint, Tanasie, 2011] some mathematical theorems and corollaries have been rigorously proven regarding the existence of an appropriate meniscus. These results are presented in Appendixes. In the following we will shown in which way the inequalities can be used for creation of the appropriate meniscus.

3.1 Convex free surface creation

In this section, it will be shown in which way the inequalities presented in Appendix 1 can be used for the creation of an appropriate static convex meniscus by the choice of p_e and p_i [Balint, Tanasie, 2011].

Inequalities (A.1.1) establish the range where the pressure difference p_e has to be chosen in order to obtain a static meniscus with convex outer free surface, appropriate for the growth of a tube of outer radius equal to $\frac{R_{ge}}{n}$.

If the pressure difference satisfies (A.1.2), then a static meniscus with convex outer free surface is obtained which is appropriate for the growth of a tube of outer radius $r_e \in \left[\frac{R_{ge}}{n}, R_{ge}\right]$.

If the pressure difference satisfies inequality (A.1.4) and the value of p_e is close to the value of the right hand member of the inequality (A.1.4) then a static meniscus with convex outer free surface is obtained which is appropriate for the growth of a tube of outer radius equal to $\frac{R_{ge} + R_{gi}}{2}$.

If the pressure difference satisfies inequality (A.1.5), then a static meniscus with convex outer free surface is obtained which is appropriate for the growth of a tube of outer radius in the range $\left[\frac{R_{ge}}{n}, \frac{R_{ge}}{n'}\right]$.

Theorem 5 (Appendix 1) shows that a static meniscus having a convex outer free surface, appropriate for the growth of a tube of outer radius r_e situated in the range $\left[\frac{R_{ge}}{n}, \frac{R_{ge}}{n'}\right]$, is stable.

Inequalities (A.1.6) establish the range where the pressure difference p_i has to be chosen in order to obtain a static meniscus with convex inner free surface appropriate for the growth of a tube of inner radius equal to $m \cdot R_{gi}$.

If the pressure difference p_i satisfies (A.1.7) then a static meniscus with convex inner free surface is obtained which is appropriate for the growth of a tube of inner radius $r_i < m \cdot R_{gi}$.

If the pressure difference p_i satisfies the inequality (A.1.9) and the value of p_i is close to the value of the right hand term of the inequality (A.1.9) then a static meniscus with convex inner free surface is obtained which is appropriate for the growth of a tube of inner radius equal to $\frac{R_{ge}+R_{gi}}{2}$.

If the pressure difference p_i satisfies inequality (A.1.10) then a static meniscus with convex inner free surface is obtained which is appropriate for the growth of a tube of inner radius which is in the range $\left[m'\cdot R_{gi}, m\cdot R_{gi}\right]$.

Theorem 10 (Appendix 1) shows that a static meniscus having a covex inner free surface appropriate for the growth of a tube of inner radius r_i situated in the range $\left[R_{gi}, \frac{R_{gi}+R_{ge}}{2}\right]$ is stable.

For numerical illustrations, the inner radius of the shaper was taken $R_{gi}=4.2\times10^{-3}$ [m] and outer radius of the shaper was chosen $R_{ge}=4.8\times10^{-3}$ [m] [Eriss, 1980]. Computations were performed in **MathCAD 14**. and for **Si** the following numerical values were considered: $\rho=2.5\times10^{3}$ [kg/m^3]; $\gamma=7.2\times10^{-1}$ [N/m]; α_c =30^o; α_g =11^o; g=9.81[m/s^2].

To create a convex meniscus appropriate for the growth of a tube having the outer radius r_e^1 equal to $r_e^1=4.65\times10^{-3}$ [m] ($n_1=1.03226$), according to the **Theorem 1** (Appendix 1), p_e has to be chosen in the range: $\left[-3480.07,-612.35\right]$ [Pa]. According to the **Corollary 3** (Appendix 1), from this range for the values of p_e smaller than -1702.52 [Pa] the point r_e where $z_e'(r_e)=-\tan\left(\pi/2-\alpha_g\right)$ is close to 4.5×10^{-3} [m]. Hence, we have to find for $p_e=-1702.52$ [Pa] the point r_e for which the above condition is satisfied. This can be made by integrating numerically the following system for $z(R_{ge})=0$, $\alpha(R_{ge})=\alpha_c$ and $p_e=-1702.52$ [Pa] (see Fig. 3):

$$\begin{cases}\dfrac{dz_e}{dr}=-\tan(\alpha_e)\\[2ex]\dfrac{d\alpha_e}{dr}=\dfrac{p_e-\rho\cdot g\cdot z_e}{\gamma}\cdot\dfrac{1}{\cos\alpha_e}-\dfrac{1}{r}\cdot\tan\alpha_e\end{cases}\tag{10}$$

Since the obtained r_e is $r_e=4.609\times10^{-3}$ [m], and it is smaller than the desired value $r_e^1=4.65\times10^{-3}$ [m], the value of p_e has to be chosen in the range $\left[-3480.07,-1702.52\right]$ [Pa].

The results of the integrations of the system (10) for $z(R_{ge})=0$, $\alpha(R_{ge})=\alpha_c$ and different values of p_e in this range, are presented in Fig. 4. This figure shows that the outer radius $r_e^1=4.65\times10^{-3}$ [m] is obtained for $p_e^1=-2198$ [Pa].

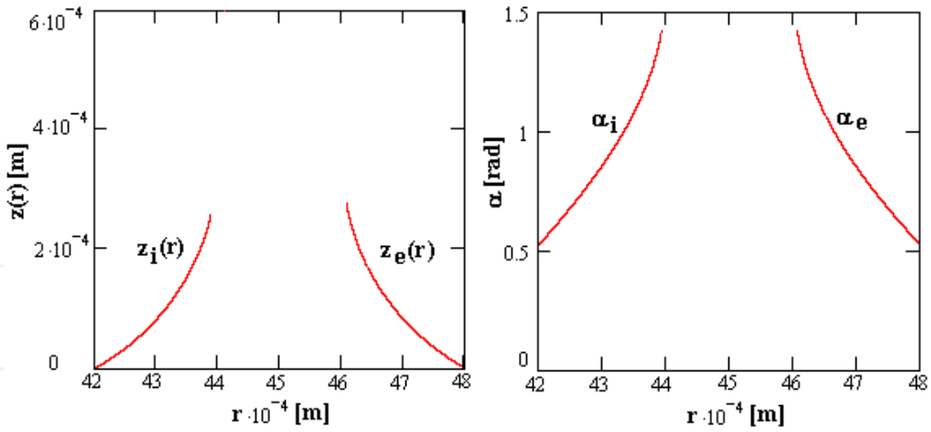

Fig. 3. The results of the integration of systems (10) and (11) for $p_e = -1702.52$ [Pa] and $p_i = -1945.80$ [Pa]

Taking $p_m \approx 0$ [Eriss et al., 1980], [Rossolenko et al., 2001], [Yang et al., 2006], the melt column height in this case is $H_e^1 = \frac{1}{\rho \cdot g}\left(2198 - p_g^e\right)$, where $p_g^e \geq 0$ is the pressure of the gas flow (introduced in the furnace for release, the heat from the outer wall of the tube). When $p_g^e = 0$, then $H_e^1 = 8.96 \times 10^{-2}$ [m] i.e. the shaper's outer top level has to be with $H_e^1 = 8.96 \times 10^{-2}$ [m] above the crucible melt level.

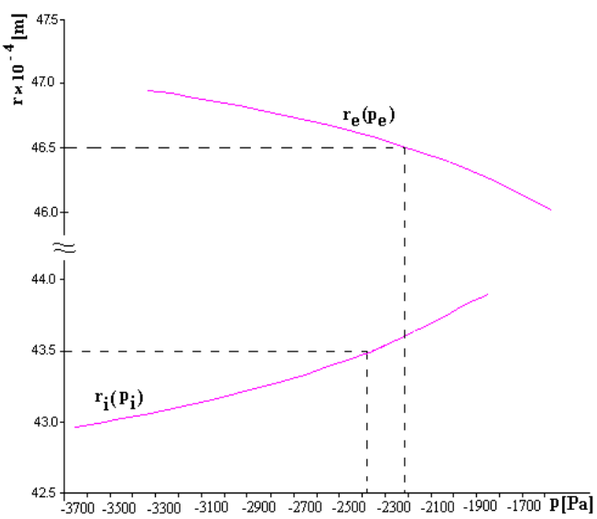

Fig. 4. The tube outer radius and inner radius versus p_e and p_i

To create a convex meniscus appropriate for the growth of a tube having the inner radius $r_i^1 = 4.35 \times 10^{-3}$ [m] ($m_1 = 1.03571$), according to the **Theorem 6** (Appendix 1), p_i has to be chosen in the range: $[-3723.32, -847.10]$ [Pa]. According to the **Corollary 8** (Appendix 1), from this range for the values of p_i smaller than -1945.80 [Pa], the point r_i where the

condition $z_i'(r_i) = \tan\left(\pi/2 - \alpha_g\right)$ is satisfied is close to 4.5×10^{-3} [m]. Therefore, we have to find now for $p_i = -1945.80$ [Pa] the point r_i where the above condition is achieved. This can be made by integrating numerically the system:

$$\begin{cases} \dfrac{dz_i}{dr} = \tan\alpha_i \\ \dfrac{d\alpha_i}{dr} = \dfrac{\rho\cdot g\cdot z_i - p_i}{\gamma}\cdot\dfrac{1}{\cos\alpha_i} - \dfrac{1}{r}\cdot\tan\alpha_i \end{cases} \tag{11}$$

for $z(R_{gi}) = 0$, $\alpha(R_{gi}) = \alpha_c$ and $p_i = -1945.80$ [Pa]. (see Fig. 3).

Since the obtained r_i is $r_i = 4.390\times10^{-3}$ [m] and it is higher than the desired value $r_i^1 = 4.35\times10^{-3}$ [m], we have to choose the value of p_i in the range $\left[-3723.32 - 1945.80\right]$ [Pa].

The results of the integrations of the system (11) for $z(R_{gi}) = 0$, $\alpha(R_{gi}) = \alpha_c$ and for different values of p_i in this range are represented in Fig. 4.

This figure shows that the inner radius $r_i^1 = 4.35\times10^{-3}$ [m] is obtained for $p_i^1 = -2434$ [Pa].

Taking $p_m \approx 0$ [Eriss et al., 1980], [Rossolenko et al., 2001], [Yang et al., 2006], the melt column height is $H_i^1 = \dfrac{1}{\rho\cdot g}\left(2434 - p_g^i\right)$, where $p_g^i \geq 0$ is the pressure of the gas flow (introduced in the furnace for releasing the heat from the inner wall of the tube). When $p_g^i = 0$, then $H_i^1 = 9.92\times10^{-2}$ [m], i.e. the shaper's inner top level has to be with $H_i^1 = 9.92\times10^{-2}$ [m] above the crucible melt level. When $p_g^i \geq 2434$, then H_i^1 is negative, i.e. the crucible melt level has to be above the shaper's inner top level.

To create a convex meniscus appropriate for the growth of a tube with the outer radius $r_e^1 = 4.65\times10^{-3}$ [m] and inner radius $r_i^1 = 4.35\times10^{-3}$ [m], when the shaper's inner top is at the same level as the shaper's outer top, we have to take: $\dfrac{1}{\rho\cdot g}\left(2198 - p_g^e\right) = \dfrac{1}{\rho\cdot g}\left(2434 - p_g^i\right)$. It follows that the pressure of the gas flow, introduced in the furnace for releasing the heat from the inner wall of the tube has to be higher than the pressure of the gas flow, introduced in the furnace for releasing the heat from the outer wall of the tube and we have to take: $p_g^i - p_g^e = 236$ [Pa].

3.2 Concave free surface creation

In this section, it will be shown in which way the inequalities presented in Appendix 2 can be used for the creation of an appropriate static concave meniscus by the choice of p_e and p_i [Balint&Balint, 2009a].

Inequalities (A.2.1) establish the range in which the pressure difference p_e has to be chosen in order to obtain a static meniscus with concave outer free surface appropriate for the growth of a tube of outer radius equal to $\frac{R_{ge}}{n}$.

If the pressure difference satisfies inequality (A.2.2) then a static meniscus with concave outer free surface is obtained which is appropriate for the growth of a tube of outer radius in the range $\left[\frac{R_{ge}}{n}, \frac{R_{ge}}{n'}\right]$.

Theorem 13 (Appendix 2) shows that a static meniscus having a concave outer free surface appropriate for the growth of a tube of outer radius $r_e \in \left[\frac{R_{gi}+R_{ge}}{2}, R_{ge}\right]$ is stable.

Inequalities (A.2.3) establish the range in which the pressure difference p_i has to be chosen in order to obtain a static meniscus with convex inner free surface appropriate for the growth of a tube of inner radius equal to $m \cdot R_{gi}$.

If the pressure difference p_i satisfies inequality (A.2.4) then a static meniscus with concave inner free surface is obtained which is appropriate for the growth of a tube of inner radius in the range $\left[m' \cdot R_{gi}, m \cdot R_{gi}\right]$.

Theorem 16 (Appendix 2) shows that a static meniscus having a concave inner free surface appropriate for the growth of a tube of inner radius $r_i \in \left[R_{gi}, \frac{R_{gi}+R_{ge}}{2}\right]$ is stable.

Computations were performed for an InSb tube growth: $\alpha_c = 63.8^0$; $\alpha_g = 28.9^0$; $\rho = 6582\left[kg/m^3\right]$; $\gamma = 4.2 \times 10^{-1}\left[N/m\right]$.

If there exists a concave outer free surface, appropriate for the growth of a tube of outer radius $r_e^1 = 4.65 \times 10^{-3}[m]$ ($n_1 = 1.03226$), then according to the **Theorem 11** (Appendix 2) this can be obtained for a value of p_e in the range $(134.85; 164.49)[Pa]$.

Taking into account the above fact, in order to create a concave outer free surface, appropriate for the growth of a tube of which outer radius is equal to $r_e^1 = 4.65 \times 10^{-3}[m]$ we have solved the i.v.p. (A.1.3) for different values of p_e in the range $(134.85; 164.49)[Pa]$.

More precisely, we have integrated the system (10) for $z_e(R_{ge}) = 0$, $z_e'(R_{ge}) = -\tan\alpha_c$ and different p_e. The obtained outer radii r_e versus p_e are represented in Fig.5, which shows that the desired outer radius $r_e^1 = 4.65 \times 10^{-3}[m]$ is obtained for $p_e' = 149.7[Pa]$.

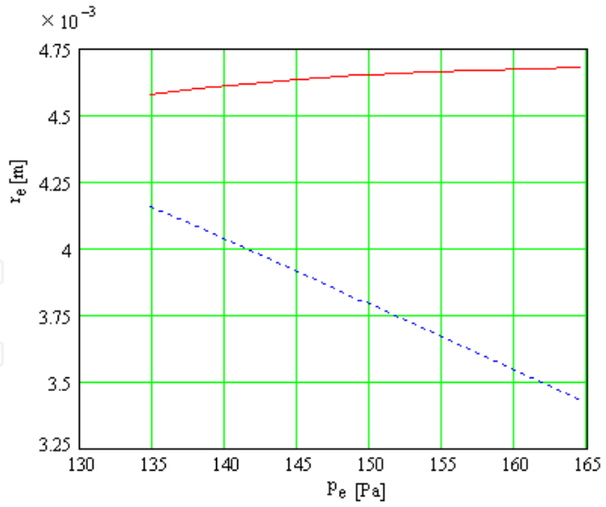

Fig. 5. Outer radii r_e versus p_e in the range $(134.85; 164.49)[Pa]$.

Actually, as it can be seen in the same figure, for $p_e' = 149.7[Pa]$ we can also obtain a second outer radius $r_e^2 = 3.8 \times 10^{-3}[m]$, which is not in the desired range $\left(\frac{R_{gi} + R_{ge}}{2}, R_{ge}\right)$. Moreover, the outer free surface of this meniscus is not globally concave; it is a convex-concave meniscus (Fig.6).

Taking into account $p_m \approx 0$ [Eriss, 1980], [Rossolenko, 2001], [Yang, 2006], the melt column height in this case is $H_e' = -\frac{1}{\rho \cdot g} \cdot [p_e' + p_g^e]$, where $p_g^e \geq 0$ is the pressure of the gas flow (introduced in the furnace for releasing the heat from the outer side of the tube wall). When $p_g^e = 0$, then H_e' is negative, $H_e' = -2.31 \times 10^{-3}[m]$, i.e. the crucible melt level has to be with $-H_e' = 2.31 \times 10^{-3}[m]$ above the shaper top level.

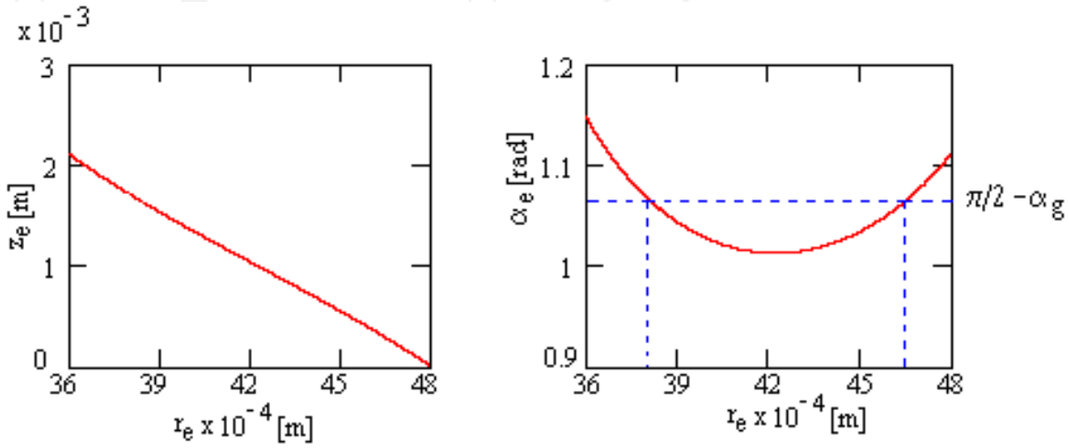

Fig. 6. Non globally concave outer free surface obtained for $p_e' = 149.7[Pa]$.

If there exists a concave inner free surface for the growth of a tube of inner radius $r_i' = 4.35\times 10^{-3}[m]$ ($m_1 = 1.03571$), then according to the **Theorem 14** (Appendix 2), this can be obtained for a value of p_i which is in the range $(-31.46, -1.07)[Pa]$.

Taking into account the above fact, in order to create a concave inner free surface, appropriate for the growth of a tube whose inner radius is equal to $r_i' = 4.35\times 10^{-3}[m]$, we have solved the i.v.p. (A.1.8) for different values of p_i in the range $(-31.46, -1.07)[Pa]$. More precisely, we have integrated the system (11) for $z_i(R_{gi}) = 0$, $z_i'(R_{gi}) = \tan\alpha_c$ and different p_i. The obtained inner radii r_i versus p_i are represented in Fig.7 which shows that the desired inner radius $r_i^1 = 4.35\times 10^{-3}[m]$ is obtained for $p_i' = -16.2[Pa]$.

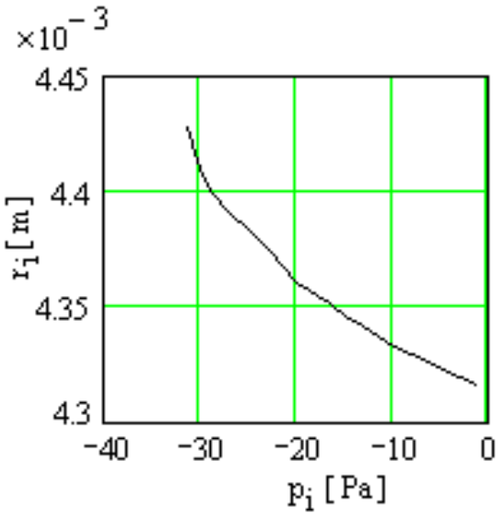

Fig. 7. Inner radii r_i versus p_i in the range $(-31.46, -1.07)[Pa]$.

Taking $p_m \approx 0$ [Eriss et al., 1980], [Rossolenko et al., 2001], [Yang et al. 2006], the melt column height in this case is $H_i' = -\frac{1}{\rho\cdot g}\cdot[p_i' + p_g^i]$, where $p_g^i \geq 0$ is the pressure of the gas flow (introduced in the furnace for releasing the heat from the inner side of the tube wall). When $p_g^i = 0$, then H_i' is positive, $H_i' = 0.25\times 10^{-3}[m]$, i.e. the crucible melt level has to be with $H_i' = 0.25\times 10^{-3}[m]$ under the shaper top level. To create a concave meniscus, appropriate for the growth of a tube with outer radius $r_e' = 4.65\times 10^{-3}$ [m] and inner radius $r_i' = 4.35\times 10^{-3}$ [m] the melt column heights (with respect to the crucible melt level) have to be $H_i^1 = -\frac{1}{\rho\cdot g}\cdot\left[-16.2 + p_g^i\right]$ and $H_e^1 = -\frac{1}{\rho\cdot g}\cdot\left[149.7 + p_g^e\right]$. When the shaper's outer top is at the same level as the shaper's inner top, with respect to the crucible melt level, then the relation $H_e^1 = H_i^1$ holds . It follows that the pressure of the gas flow, introduced in the

furnace for releasing the heat from the inner wall of the tube, p_g^i has to be higher than the pressure of the gas flow introduced in the furnace for releasing the heat from the outer wall of the tube, p_g^e; $p_g^i - p_g^e = 149.7 + 16.2 = 165.9[Pa]$.

4. The angles $\bar{\alpha}_e(r_e, h_e, p_e)$ and $\bar{\alpha}_i(r_i, h_i, p_i)$ which appear in system (1) describing the dynamics of the outer and inner radius of a tube, grown by the E.F.G. technique

4.1 The procedure for the determination of the angles $\bar{\alpha}_e(r_e, h_e, p_e)$ and $\bar{\alpha}_i(r_i, h_i, p_i)$ for a convex free surface

The angles $\bar{\alpha}_e(r_e, h_e, p_e)$ ($\bar{\alpha}_i(r_i, h_i, p_i)$) represent the angles between the tangent line to the outer free surface (inner free surface) of the meniscus at the three phase point, of coordinates (r_e, h_e) $((r_i, h_i))$ and the horizontal axis Or. These angles can fluctuate during the growth. The deviation of the tangent to the crystal outer (inner) free surface at the triple point from the vertical is the difference $\bar{\alpha}_e(r_e, h_e, p_e) - \left(\frac{\pi}{2} - \alpha_g\right)$, $\left(\bar{\alpha}_i(r_i, h_i, p_i) - \left(\frac{\pi}{2} - \alpha_g\right)\right)$ (Fig. 2), where α_g is the growth angle. The deviation can fluctuate also and the outer (inner) radius r_e (r_i) is constant when the deviation is constant equal to zero

The angles $\bar{\alpha}_e(r_e, h_e, p_e)$ and $\bar{\alpha}_i(r_i, h_i, p_i)$ cannot be obtained directly from the Young-Laplace equation. For this reason for this equation the following strategy is adopted: two conditions are imposed at the outer radius R_{ge} of the shaper (inner radius R_{gi} of the shaper) $z_e(R_{ge}) = 0$; $z_e'(R_{ge}) = -\tan(\alpha_c^e)$ ($z_i(R_{gi}) = 0$, $z_i'(R_{gi}) = \tan(\alpha_c^i)$). In the last condition α_c^e (α_c^i) is a parameter which can fluctuate in a certain range, during the growth. For different values of α_c^e (α_c^i) in a given range the solution $z_e(r; \alpha_c^e, p_e)$ ($z_i(r; \alpha_c^i, p_i)$) of the Young-Laplace equation which satisfies the conditions $z_e(R_{ge}) = 0$; $z_e'(R_{ge}) = -\tan(\alpha_c^e)$ at R_{ge} (($z_i(R_{gi}) = 0$, $z_i'(R_{gi}) = \tan(\alpha_c^i)$) at R_{gi}) is found.

With $z_e(r; \alpha_c^e, p_e)$ ($z_i(r; \alpha_c^i, p_i)$) the function $\alpha_e(r_e; \alpha_c^e, p_e) = -\arctan z_e'(r_e; \alpha_c^e, p_e)$ ($\alpha_i(r_i; \alpha_c^i, p_i) = \arctan z_i'(r_i; \alpha_c^i, p_i)$) is constructed. After that, from $h_e = z_e(r; \alpha_c^e, p_e)$ ($h_i = z_i(r; \alpha_c^i, p_i)$) α_c^e (α_c^i) is expressed as function of r_e, h_e and p_e (r_i, h_i and p_i).

$\alpha_c^e = \alpha_c^e(r_e; h_e, p_e)$ ($\alpha_c^i = \alpha_c^i(r_i; h_e, p_i)$) is introduced in $\alpha_e(r_e; \alpha_c^e, p_e)$ ($\alpha_i(r_i; \alpha_c^i, p_i)$) obtaining the function

$$\bar{\alpha}_e(r_e, h_e, p_e) = \alpha_e(r_e; \alpha_c^e(r_e; h_e, p_e), p_e) \qquad (\bar{\alpha}_i(r_i, h_i, p_i) = \alpha_i(r_i; \alpha_c^i(r_i; h_i, p_i), p_i)).$$

To the best of our knowledge, there is no algorithm in the literature concerning the construction of $\bar{\alpha}_e(r_e, h_e, p_e)$ ($\bar{\alpha}_i(r_i, h_i, p_i)$) at the level of generality presented here.

Due to the nonlinearity, the above described procedure can't be realized analytically. This is the reason why for the construction of the function $\bar{\alpha}_e(r_e;\alpha_c,p_e)$ in [Balint&Tanasie, 2010] the following numerical procedure was conceived:

Step 1. For a given α_c^{e0}; $\alpha_c^{e0}\in\left(0,\pi/2-\alpha_g\right)$ and $n=\dfrac{2\cdot R_{ge}}{R_{ge}+R_{gi}}$ an $n'\in(1,n)$ is found such that $E_1^e\left(n',\alpha_c^{e0}\right)<E_2^e\left(n,\alpha_c^{e0}\right)$ where:

$$E_1^e\left(n',\alpha_c^{e0}\right)=-\gamma\cdot\frac{\pi/2-\left(\alpha_c^{e0}+\alpha_g\right)}{R_{ge}}\cdot\frac{n'}{n'-1}\cdot\sin\alpha_g+\rho_1\cdot g\cdot R_{ge}\cdot\frac{n'-1}{n'}\cdot\tan\left(\pi/2-\alpha_g\right)+$$
$$+\frac{\gamma}{R_{ge}}\cdot n'\cdot\cos\alpha_g \qquad (12)$$
$$E_2^e(n,\alpha_c^{e0})=-\gamma\cdot\frac{\pi/2-\left(\alpha_c^{e0}+\alpha_g\right)}{R_{ge}}\cdot\frac{n}{n-1}\cdot\cos\alpha_c^{e0}+\frac{\gamma}{R_{ge}}\cdot\sin\alpha_c^{e0}$$

Step 2. For α_c^e a range $\left[\underline{\alpha}_c^e,\overline{\alpha}_c^e\right]$ is determined such that $0<\underline{\alpha}_c^e<\alpha_c^{e0}<\overline{\alpha}_c^e<\pi/2-\alpha_g$ and for every $\alpha_c^e\in\left[\underline{\alpha}_c^e,\overline{\alpha}_c^e\right]$ the inequality $E_1^e\left(n',\alpha_c^e\right)<E_2^e\left(n,\alpha_c^e\right)$ holds.

Step 3. For p_e the range $\left[\underline{p}_e,\overline{p}_e\right]$ defined by:

$$\underline{p}_e=\sup_{\alpha_c^e\in\left[\underline{\alpha}_c^e,\overline{\alpha}_c^e\right]}E_1^e\left(n',\alpha_c^e\right)\qquad\qquad \overline{p}_e=\inf_{\alpha_c^e\in\left[\underline{\alpha}_c^e,\overline{\alpha}_c^e\right]}E_2^e\left(n,\alpha_c^e\right) \qquad (13)$$

is considered.

Step 4. In the range $\left[\underline{\alpha}_c^e,\overline{\alpha}_c^e\right]$ a set of l different values of α_c^e is chosen.

Step 5. In the range $\left[\underline{p}_e,\overline{p}_e\right]$ a set of m different values of p_e is chosen.

Step 6. In a given range $\left[\underline{\alpha}_e,\overline{\alpha}_e\right]$ possessing the property $\overline{\alpha}_c^e<\underline{\alpha}_e<\pi/2-\alpha_g<\overline{\alpha}_e<\pi/2$ a set of j values of α_e is chosen: $\underline{\alpha}_e=\alpha_e^1<\alpha_e^2<\ldots<\alpha_e^j=\overline{\alpha}_e$.

Step 7. For a given p_e^k, $k=\overline{1,m}$ and α_c^{eq}, $q=\overline{1,l}$ the solution of the system (10) corresponding to the conditions: $z_e(R_{ge})=0$, $\alpha_e(R_{ge})=\alpha_c^{eq}$ is determined numerically obtaining the functions (profiles curves Refs [Tatarchenko, 1993]): $z_e=z_e(r;\alpha_c^{eq},p_e^k)$ and $\alpha_e=\alpha_e(r;\alpha_c^{eq},p_e^k)$.

Step 8. The values $r_{k\,q\,s}^e$ for which $\alpha_e(r_{k\,q\,s}^e;\alpha_c^{eq},p_e^k)=\alpha_e^s\in\left[\underline{\alpha}_e,\overline{\alpha}_e\right]$, $k=\overline{1,m}$, $q=\overline{1,l}$ are determined.

Step 9. The values $h^e_{kqs} = z_e(r^e_{kqs}; \alpha^{eq}_c, p^k_e)$ are found.

Step 10. Fitting the data r^e_{kqs} h^e_{kqs} p^k_e and α^s_e, the function $\bar{\alpha}_e(r_e, h_e, p_e)$ is found.

For the same reason as in the case of $\bar{\alpha}_e(r_e, h_e, p_e)$ for the construction of $\bar{\alpha}_i = \bar{\alpha}_i(r_i, h_i, p_i)$ the following numerical procedure was conceived:

Step 1. For $\alpha^{i0}_c = \alpha^{e0}_c$ and $m \in \left(1, \dfrac{R_{ge} + R_{gi}}{2 \cdot R_{gi}}\right]$ an $m' \in (1, m)$ is determined such that $E^i_1\left(m', \alpha^{i0}_c\right) < E^i_2\left(m, \alpha^{i0}_c\right)$ where:

$$E^i_1\left(m', \alpha^{i0}_c\right) = -\gamma \cdot \frac{\pi/2 - \left(\alpha^{i0}_c + \alpha_g\right)}{(m'-1) \cdot R_{gi}} \cdot \sin\alpha_g + \rho_1 \cdot g \cdot R_{gi} \cdot (m'-1) \cdot \tan\left(\pi/2 - \alpha_g\right) - \\ - \frac{\gamma}{m' \cdot R_{gi}} \cdot \sin\alpha^{i0}_c \tag{14}$$

$$E^i_2(m, \alpha^{i0}_c) = -\gamma \cdot \frac{\pi/2 - \left(\alpha^{i0}_c + \alpha_g\right)}{(m-1) \cdot R_{gi}} \cdot \cos\alpha^{i0}_c - \frac{\gamma}{R_{gi}} \cdot \cos\alpha_g$$

Step 2. For α^i_c a range $\left[\underline{\alpha}^i_c, \overline{\alpha}^i_c\right]$ is determined such that $0 < \underline{\alpha}^i_c < \alpha^i_c < \overline{\alpha}^i_c < \pi/2 - \alpha_g$ and for every $\alpha^i_c \in \left[\underline{\alpha}^i_c, \overline{\alpha}^i_c\right]$, the inequality $E^i_1\left(m', \alpha^i_c\right) < E^i_2\left(m, \alpha^i_c\right)$ holds.

Step 3. For p_i the range $\left[\underline{p}_i, \overline{p}_i\right]$ defined by:

$$\underline{p}_i = \sup_{\alpha^i_c \in \left[\underline{\alpha}^i_c, \overline{\alpha}^i_c\right]} E^i_1\left(m', \alpha^i_c\right) \qquad \overline{p}_i = \inf_{\alpha^i_c \in \left[\underline{\alpha}^i_c, \overline{\alpha}^i_c\right]} E^i_2\left(m, \alpha^i_c\right) \tag{15}$$

is considered.

Step 4. In the range $\left[\underline{\alpha}^i_c, \overline{\alpha}^i_c\right]$ a set of l different values of α^i_c are chosen.

Step 5. In the range $\left[\underline{p}_i, \overline{p}_i\right]$ a set of n different values of p_i are chosen.

Step 6. In a given range $\left[\underline{\alpha}_i, \overline{\alpha}_i\right]$, possessing the property $\overline{\alpha}^i_c < \underline{\alpha}_i < \pi/2 - \alpha_g < \overline{\alpha}_i < \pi/2$, a set of j values of α_i are chosen: $\underline{\alpha}_i = \alpha^1_i < \alpha^2_i < \ldots < \alpha^j_i = \overline{\alpha}_i$.

Step 7. For a given p^k_i, $k = \overline{1,n}$ and α^{iq}_c, $q = \overline{1,l}$ the solution of the system (11) which satisfies the conditions: $z_i(R_{gi}) = 0$, $\alpha_i(R_{gi}) = \alpha^{iq}_c$ is found numerically obtaining the functions (profiles curves Ref. [Tatarchenko, 1993]): $z_i = z_i(r; \alpha^{iq}_c, p^k_i)$ and $\alpha_i = \alpha_i(r; \alpha^{iq}_c, p^k_i)$.

Step 8. The values $r^i_{k\,q\,s}$ for which $\alpha_i(r^i_{k\,q\,s};\alpha^{iq}_c,p^k_i)=\alpha^s_i\in\left[\underline{\alpha}_e,\overline{\alpha}_e\right]$, $k=\overline{1,n}$, $q=\overline{1,l}$ are determined.

Step 9. The values $h^i_{kqs}=z_i(r^i_{kqs};\alpha^{iq}_c,p^k_i)$ are found.

Step 10. The function $\bar{\alpha}_i(r_i,h_i,p_i)$ is found by fitting the data r^i_{kqs} h^i_{kqs} p^k_i and α^s_i.

For the case of a silicon tube and the outer free surface the function:

$$\bar{\alpha}_e(r_e,h_e,p_e)=\frac{a_1(p_e)+a_2(p_e)\cdot r_e+a_3(p_e)\cdot r_e^2+a_4(p_e)\cdot h_e+a_5(p_e)\cdot h_e^2+a_6(p_e)\cdot h_e^3}{1+a_7(p_e)\cdot r_e+a_8(p_e)\cdot h_e+a_9(p_e)\cdot h_e^2+a_{10}(p_e)\cdot h_e^3}$$

with: $a_1(p_e)=0.400314546-0.00494101\cdot \mathrm{p_e}$ $a_2(p_e)=-374.789455+2.353132518\cdot \mathrm{p_e}$

$a_3(p_e)=56161.27414-244.013259\cdot \mathrm{p_e}$ $a_4(p_e)=393.2446055+0.010192507\cdot \mathrm{p_e}$

$a_5(p_e)=91143.39025-555.405995\cdot \mathrm{p_e}$ $a_6(p_e)=-1097500000-1168100\cdot \mathrm{p_e}$

$a_7(p_e)=-200.489376+0.001998751\cdot \mathrm{p_e}$ $a_8(p_e)=114.0391478+0.002922594\cdot \mathrm{p_e}$

$a_9(p_e)=83485.77784-477.770821\cdot \mathrm{p_e}$ $a_{10}(p_e)=415910000+476372.6048\cdot \mathrm{p_e}$

was obtained and for the inner free surface the function:

$$\bar{\alpha}_i(r_i;h_i,p_i)=\frac{b_1(p_i)+b_2(p_i)\cdot r_i+b_3(p_i)\cdot r_i^2+b_4(p_i)\cdot h_i+b_5(p_i)\cdot h_i^2+b_6(p_i)\cdot h_i^3}{1+b_7(p_i)\cdot r_i+b_8(p_i)\cdot h_i+b_9(p_i)\cdot h_i^2+b_{10}(p_i)\cdot h_i^3}$$

with $b_1(p_i)=0.102617985+0.004931999\cdot \mathrm{p_i}$ $b_2(p_i)=-172.7251-2.34898717\cdot \mathrm{p_i}$

$b_3(p_i)=29313.52855+277.5275727\cdot \mathrm{p_i}$ $b_4(p_i)=444.327355+0.367481455\cdot \mathrm{p_i}$

$b_5(p_i)=-2687700-817.408936\cdot \mathrm{p_i}$ $b_6(p_i)=5760710000+3810000\cdot \mathrm{p_i}$

$b_7(p_i)=-263.39243-0.00872161\cdot \mathrm{p_i}$ $b_8(p_i)=707.770183+0.334375383\cdot \mathrm{p_i}$

$b_9(p_i)=-2709500-696.727273\cdot \mathrm{p_i}$ $b_{10}(p_i)=3090180000+1348660\cdot \mathrm{p_i}$

was obtained. For $p_e=-2000[Pa]$ and $p_i=-2242[Pa]$ the functions $\bar{\alpha}_e(r_e,h_e,p_e)$ and $\bar{\alpha}_i(r_i,h_i,p_i)$ are represented in Fig. 8.:

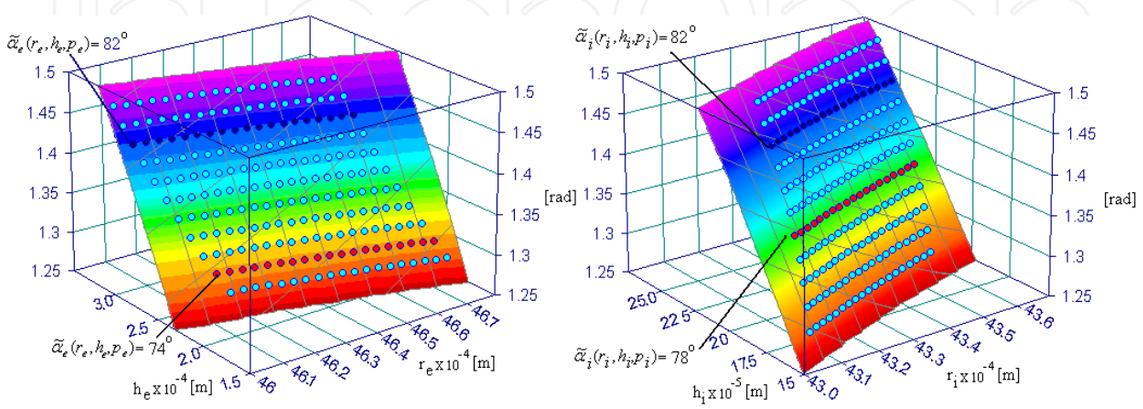

Fig. 8. The graphics of $\bar{\alpha}_e(r_e,h_e,p_e)$ ($p_e=-2000[Pa]$) and $\bar{\alpha}(r_i,h_i,p_i)$ ($p_i=-2242[Pa]$)

4.2 The procedure for the determination of the angles $\bar{\alpha}_e(r_e,h_e,p_e)$ and $\bar{\alpha}(r_i,h_i,p_i)$ for a concave free surface

The numerical procedure for the construction of the function $\bar{\alpha}_e(r_e,h_e,p_e)$ for a concave free surface (when $\alpha_c > \frac{\pi}{2}-\alpha_g$) is similar to those applied for a convex free surface. Only **Step 1-Step 3**. present the some differences. For the outer free surface we have to consider:

Step 1. For a given α_c^{e0}; $\alpha_c^{e0} \in \left(\pi/2-\alpha_g, \pi/2\right)$ and $n = \frac{2\cdot R_{ge}}{R_{ge}+R_{gi}}$ an $n' \in (1,n)$ is found such that $E_1^e\left(n,\alpha_c^{e0}\right) < E_2^e\left(n',\alpha_c^{e0}\right)$ where:

$$E_1^e\left(n,\alpha_c^{e0}\right) = \gamma\cdot\frac{\alpha_c^{e0}+\alpha_g-\pi/2}{R_{ge}}\cdot\frac{n}{n-1}\cdot\sin\alpha_g + \rho_1\cdot g\cdot R_{ge}\cdot\frac{n-1}{n}\cdot\tan\alpha_c^{e0} + \frac{\gamma}{R_{ge}}\cdot n\cdot\sin\alpha_c^{e0}$$
$$E_2^e(n',\alpha_c^{e0}) = \gamma\cdot\frac{\alpha_c^{e0}+\alpha_g-\pi/2}{R_{ge}}\cdot\frac{n'}{n'-1}\cdot\cos\alpha_c^{e0} + \frac{\gamma}{R_{ge}}\cdot\cos\alpha_g \qquad (16)$$

Step 2. For α_c^e a range $\left[\underline{\alpha}_c^e, \bar{\alpha}_c^e\right]$ is determined such that $\pi/2-\alpha_g < \underline{\alpha}_c^e < \alpha_c^{e0} < \bar{\alpha}_c^e < \pi/2$ and the inequality $\sup_{\alpha_c^e\in\left[\underline{\alpha}_c^e,\bar{\alpha}_c^e\right]} E_1^e\left(n,\alpha_c^e\right) < \inf_{\alpha_c^e\in\left[\underline{\alpha}_c^e,\bar{\alpha}_c^e\right]} E_2^e\left(n',\alpha_c^e\right)$ holds.

Step 3. For p_e the range $\left[\underline{p}_e, \bar{p}_e\right]$ defined by:

$$\underline{p}_e = \sup_{\alpha_c^e\in\left[\underline{\alpha}_c^e,\bar{\alpha}_c^e\right]} E_1^e\left(n,\alpha_c^e\right) \qquad \bar{p}_e = \inf_{\alpha_c^e\in\left[\underline{\alpha}_c^e,\bar{\alpha}_c^e\right]} E_2^e\left(n',\alpha_c^e\right) \qquad (17)$$

is considered.

For the inner free surface we have to make:

Step 1. For $\alpha_c^{i0} = \alpha_c^{e0}$ and $m \in \left(1, \frac{R_{ge}+R_{gi}}{2\cdot R_{gi}}\right]$ an $m' \in (1,m)$ is determined such that $E_1^i\left(m,\alpha_c^{i0}\right) < E_2^i\left(m',\alpha_c^{i0}\right)$ where:

$$E_1^i\left(m,\alpha_c^{i0}\right) = \gamma\cdot\frac{\alpha_c^{i0}+\alpha_g-\pi/2}{(m-1)\cdot R_{ge}}\cdot\sin\alpha_g + \rho_1\cdot g\cdot R_{gi}\cdot(m-1)\cdot\tan\alpha_c^{i0} - \frac{\gamma}{m\cdot R_{gi}}\cdot\cos\alpha_g$$
$$E_2^i(m',\alpha_c^{i0}) = \gamma\cdot\frac{\alpha_c^{i0}+\alpha_g-\pi/2}{(m'-1)\cdot R_{gi}}\cdot\cos\alpha_c^{i0} + \frac{\gamma}{R_{gi}}\cdot\sin\alpha_c^{i0} \qquad (18)$$

Step 2. For α_c^i a range $\left[\underline{\alpha}_c^i, \bar{\alpha}_c^i\right]$ is determined such that $\pi/2-\alpha_g < \underline{\alpha}_c^i < \alpha_c^{i0} < \bar{\alpha}_c^i < \pi/2$ and the inequality $\sup_{\alpha_c^i\in\left[\underline{\alpha}_c^i,\bar{\alpha}_c^i\right]} E_1^i\left(m,\alpha_c^i\right) < \inf_{\alpha_c^i\in\left[\underline{\alpha}_c^i,\bar{\alpha}_c^i\right]} E_2^i\left(m',\alpha_c^i\right)$ holds.

Step 3. For p_i the range $\left[\underline{p}_i, \overline{p}_i\right]$ defined by:

$$\underline{p}_i = \sup_{\alpha_c^i \in \left[\underline{\alpha}_c^i, \overline{\alpha}_c^i\right]} E_1^i\left(m, \alpha_c^i\right) \qquad \overline{p}_i = \inf_{\alpha_c^i \in \left[\underline{\alpha}_c^i, \overline{\alpha}_c^i\right]} E_2^i\left(m', \alpha_c^i\right) \tag{19}$$

is considered.

In the case of of the InSb tube considered in section 2.2, for the outer free surface the function:

$$\overline{\alpha}_e\left(r_e, h_e, p_e\right) = \frac{a_1(p_e) + a_2(p_e)\cdot r_e + a_3(p_e)\cdot r_e^2 + a_4(p_e)\cdot h_e + a_5(p_e)\cdot h_e^2 + a_6(p_e)\cdot h_e^3}{1 + a_7(p_e)\cdot r_e + a_8(p_e)\cdot h_e + a_9(p_e)\cdot h_e^2 + a_{10}(p_e)\cdot h_e^3}$$

with
$a_1(p_e) = 16.95005004 - 0.1803412\cdot p_e$ $\quad a_2(p_e) = -6991.91018 + 76.11771837\cdot p_e$
$a_3(p_e) = 721251.8226 - 8031.90955\cdot p_e$ $\quad a_4(p_e) = 82.08229042 - 1.41357516\cdot p_e$
$a_5(p_e) = -820223.151 + 11947.58366\cdot p_e$ $\quad a_6(p_e) = 75949100 - 3370800\cdot p_e$
$a_7(p_e) = -207.085329 - 0.00600066\cdot p_e$ $\quad a_8(p_e) = 0.10447655 - 0.82800845\cdot p_e$
$a_9(p_e) = -544970.373 + 8774.44\cdot p_e$ $\quad a_{10}(p_e) = -237870000 - 663676.426\cdot p_e$

was obtained. For the inner free surface the function:

$$\overline{\alpha}_i\left(r_i; h_i, p_i\right) = \frac{b_1(p_i) + b_2(p_i)\cdot r_i + b_3(p_i)\cdot h_i + b_4(p_i)\cdot h_i^2 + b_5(p_i)\cdot h_i^3}{1 + b_6(p_i)\cdot r_i + b_7(p_i)\cdot r_i^2 + b_8(p_i)\cdot h_i + b_9(p_i)\cdot h_i^2}$$

with
$b_1(p_i) = \text{-}0.03323515 + 0.0000618675\cdot \mathrm{p_i}$ $\quad b_2(p_i) = 7.907785322\text{-}0.01471419\cdot \mathrm{p_i}$
$b_3(p_i) = \text{-}10.9920301 + 0.019065783\cdot \mathrm{p_i}$ $\quad b_4(p_i) = 81321.53642 + 10.42303935\cdot \mathrm{p_i}$
$b_5(p_i) = \text{-}6164200\text{-}109065.464\cdot \mathrm{p_i}$ $\quad b_6(p_i) = \text{-}478.279159 + 0.004407571\cdot \mathrm{p_i}$
$b_7(p_i) = 57185.4894\text{-}1.04591888\cdot \mathrm{p_i}$ $\quad b_8(p_i) = \text{-}7.40209299 + 0.012781953\cdot \mathrm{p_i}$
$b_9(p_i) = 57826.05599 + 9.103117035\cdot \mathrm{p_i}$

was obtained. For $p_e = 180[Pa]$ and $p_i = 290[Pa]$ the functions $\overline{\alpha}_e(r_e, h_e, p_e)$ and $\overline{\alpha}_i(r_i, h_i, p_i)$ are represented in Fig. 9:

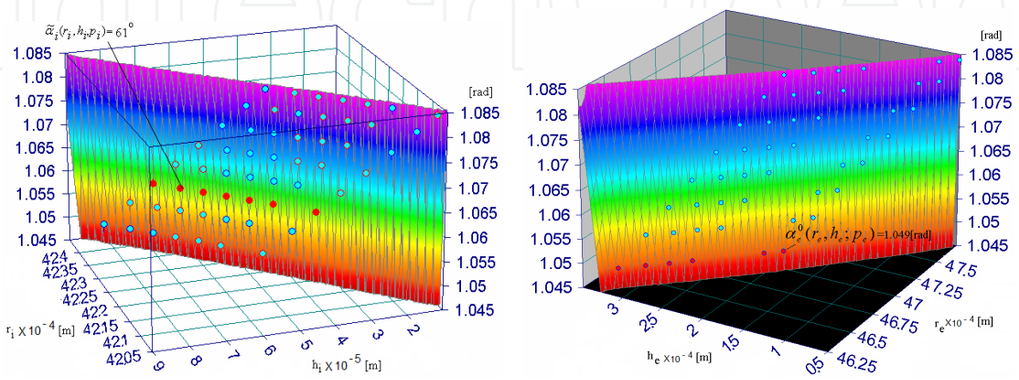

Fig. 9. The graphics of $\overline{\alpha}_i(r_i, h_i, p_i)$ $(p_i = 290[Pa])$ and $\overline{\alpha}_i(r_i, h_i, p_i)$ $(p_e = 180[Pa])$

5. Setting the pulling rate, the thermal and capillary conditions

In this section it will be shown that the results presented in the above sections can be used for setting the pulling rate, the thermal and capillary conditions in view of an experiment [Tanasie&Balint, 2010].

According to [Tatarchenko, 1993] at the level of the crystallization front h the crystallization rate v_c^j is given by:

$$v_c^j = \frac{1}{\Lambda \cdot \rho_1} \cdot \left[\lambda_1 \cdot G_1^j(r_e, r_i, h) - \lambda_2 \cdot G_2^j(r_e, r_i, h) \right], j = 1,2,3. \tag{20}$$

The difference between the pulling rate v and the crystallization rate v_c^j is equal to the crystallization front displacement rate $\frac{dh^j}{dt}$, $j = 1,2,3$.

In order to keep the crystallization front level h^j constant, the pulling rate and the thermal conditions have to satisfy the following conditions:

$$v - \frac{1}{\Lambda \cdot \rho_1} \cdot \left[\lambda_1 \cdot G_1^j(r_e, r_i, h) - \lambda_2 \cdot G_2^j(r_e, r_i, h) \right] = 0, j = 1,2,3 \tag{21}$$

When the radii r_e, r_i and the length L of the tube, which has to be grown, are prior given, and h is known, then the condition (21) can be regarded as an equation in which the pulling rate v is unknown. If this equation has a positive solution v, it depends on the following parameters: h, $T_{en}(0)$, T_0, and k. The setting of the pulling rate, thermal conditions means the choice of v, $T_{en}(0)$, T_0 and k such that the following conditions be satisfied:

- $300 < T_{en}(0) < T_m < T_0$; $0 < k < \frac{T_{en}(0) - 300}{L}$;
- equation (21) has a positive solution v in an acceptable range.
- v is practically the same for every L': $L_0 \le L' \le L$ (L_0 = the seed length).

The setting of the capillary condition means to take the tube radii r_e, r_i (prior given) and the crystallization front level h_c, determined form (21) (for the above chosen v, $T_{en}(0)$, T_0, k) and find the pressures p_e, p_i solving the followings equations:

$$\overline{\alpha}_e(r_e, h_c, p_e) = \pi/2 - \alpha_g \text{ and } \overline{\alpha}_i(r_i, h_c, p_i) = \pi/2 - \alpha_g \tag{22}$$

If the solutions p_e, p_i of this equations are in the range for which $\overline{\alpha}_e$, $\overline{\alpha}_i$ was build up, then the values p_e, p_i will be used to set p_g^e, p_g^i, H_e, H_i using (2) with $p_m = 0$ or

$$H_e = -\frac{p_g^e + p_e}{\rho_1 \cdot g}, \; H_i = -\frac{p_g^i + p_i}{\rho_1 \cdot g} \tag{23}$$

For the growth of a silicon tube with convex profile curves the following numerical data will be used: $\rho_1 = 2.5\times10^3$ [kg/m^3]; $\rho_2 = 2.3\times10^3$ [kg/m^3]; $T_m = 1683$ [K]; $\lambda_1 = 60$ [W/m·K]; $\lambda_2 = 21.6$ [W/m·K]; $\Lambda = 1.81\times10^6$ [J/kg]; $\chi_1 = \dfrac{\lambda_1}{c_1\cdot\rho_1}$; $\chi_2 = \dfrac{\lambda_2}{c_2\cdot\rho_2}$; $c_1 = 913$ [J/kg·K]; $c_2 = 703$ [J/kg·K]; $\mu_1 = 7300.42$ [K]; $\mu_2 = 2822.58$ [K]; $R_{gi} = 4.2\times10^{-3}$ [m]; $R_{ge} = 4.8\times10^{-3}$ [m]; $R_i^c = 4.339\times10^{-3}$ [m]; $R_e^c = 4.66\times10^{-3}$ [m]; $L_1 = 0.4$ [m]; $L_2 = 0.2$ [m]; $L_3 = 0.1$ [m].

Step 1. A stable static outer meniscus is chosen, whose characteristic parameters r_e, h, p_e are in the range where $\overline{\alpha}_e(r_e,h,p_e)$ is valid and for which r_e is close to r_e^c. In the case considered here such a static meniscus is obtained for $p_e = -1980$ [Pa] and its characteristic parameters are: $r_e = 4.660112250074\times10^{-3}$ [m] and $h = 2.14370857185\times10^{-4}$ [m].

Step 2. An initial input for T_0, $T_{en}(0)$ and k has to be chosen. For T_0, the start can be $T_0 = T_m + 1$. Concerning $T_{en}(0)$ and k the start can be $T_{en}(0) = T_m - 1$ and $k = \dfrac{T_{en}(0) - 300}{L}$.

Using this input and the values r_e, h, r_i^c the value of the pulling rates $v_1, v_2, \ldots, v_{40}$ given by the equation (21) have to be found. If all these values are positive, then: if the average $\overline{v}$ and standard deviation σ of the set of values of v, are acceptable, then the average pulling rate $\overline{v}$ and the initial input thermal conditions can be set, else the initial input thermal conditions have to be reset lowering in general $T_{en}(0)$ and/or increasing T_0.

Step 3. Consider $\overline{v}$, $T_{en}(0)$, T_0, k obtained above and solve equation (22) for these values choosing $r_e = r_e^c$ and $r_i = r_i^c$ (the desired radii) and h unknown. Denote by h_c the obtained solution. Replace r_e^c, r_i^c, h_c in equation (23) and solve this equations finding p_e, p_i.

Step 4. Using p_e, p_i find $H_i - H_e$, for $p_g^e = p_g^i$ (in the case of an open crucible) or find $p_g^i - p_g^e$ for $H_i - H_e = 0$ (in the case of a closed crucible).

Following the above steps for the considered silicon tube growth, some of the computed possible settings, are presented in Table 1.

For the above settings the growth process stability analysis is made through the system of nonlinear ordinary differential equations (1) which governs the evolution of r_e, r_i, h for the established settings. It means to verify first of all that the desired r_e^c, r_i^c and the obtained h_c is a steady state of (1).

Furthermore to verify if at the start r_e^c, r_i^c, h_c are perturbed (i.e. the seed sizes are different from r_e^c, r_i^c) after a period of transition the values r_e^c, r_i^c, h_c are recovered. In other words,

to verify if the steady state (r_e^c, r_i^c, h_c) is asymptotically stable. This last requirement is satisfied if the Hurwitz conditions are satisfied [Tatarchenko, 1993] i.e.:

$$\begin{gathered} -a_{11}-a_{22}-a_{33}>0,\ -a_{11}a_{22}a_{33}+a_{31}a_{13}a_{22}>0 \\ (-a_{11}-a_{22}-a_{33})(-a_{31}a_{13}+a_{11}a_{22}+a_{22}a_{33}+a_{11}a_{33})-(-a_{11}a_{22}a_{33}+a_{31}a_{13}a_{22})>0 \end{gathered} \tag{24}$$

$$\begin{gathered} a_{11}=-v\cdot\frac{\partial\bar{\alpha}_e(r_e^c,h_c,p_e)}{\partial R_e}\quad a_{12}=-v\cdot\frac{\partial\bar{\alpha}_e(r_e^c,h_c,p_e)}{\partial R_i}=0\quad a_{13}=-v\cdot\frac{\partial\bar{\alpha}_e(r_e^c,h_c,p_e)}{\partial h} \\ a_{21}=v\cdot\frac{\partial\bar{\alpha}_i(r_i^c,h_c,p_i)}{\partial R_e}=0\quad a_{22}=v\cdot\frac{\partial\bar{\alpha}_i(r_i^c,h_c,p_i)}{\partial R_i}\quad a_{23}=v\cdot\frac{\partial\bar{\alpha}_i(r_i^c,h_c,p_i)}{\partial h} \\ a_{31}=\frac{\partial S(r_e^c,r_i^c,h_c)}{\partial R_e}\qquad a_{32}=\frac{\partial S(r_e^c,r_i^c,h_c)}{\partial R_i}\quad a_{33}=\frac{\partial S(r_e^c,r_i^c,h_c)}{\partial h} \\ S(r_e,r_i,h)=\bar{v}-\frac{1}{\Lambda\cdot\rho_1}\cdot\left[\lambda_1\cdot G_1(r_e,r_i,h)-\lambda_2\cdot G_2(r_e,r_i,h)\right] \end{gathered} \tag{25}$$

	F_1	F_2	F_3		F_1	F_2	F_3
$\bar{v}$	$8.32993\cdot10$	8.29566×10	$8.29107\ \times10$	H_i-H_e	1.10328×10^{-2}	1.10320×10^{-2}	1.10324×10^{-2}
T_0	1716.46	2110.76	2933.32	$p_g^i-p_g^e$	-270.58	-270.56	-270.57
$T_{en}(0)$	400.00	400.00	400.00	h_c	2.14380×10^{-4}	2.14324×10^{-4}	2.14371×10^{-4}
k	250.00	500.00	1000.00	r_e^c	4.66000×10^{-3}	4.65990×10^{-3}	4.65990×10^{-3}
p_e	-1981.44	-1982.93	-1981.61	r_i^c	4.33900×10^{-3}	4.33900×10^{-3}	4.33899×10^{-3}
p_i	-2252.02	-2253.49	-2252.18				

Table 1. Possible settings of $\bar{v}$, T_0, $T_{en}(0)$, p_e, p_i, $p_g^i-p_g^e$

	a_{11}	a_{13}	a_{22}	a_{23}	a_{31}	a_{32}	a_{33}
F_1	-0.20278	-0.29136	-0.1984	0.285445	121.8176	0	-2534.0535
F_2	-0.20191	-0.29033	-0.19755	0.284434	27285.12	-27215.77	-42171.2316
F_3	-0.20183	-0.29002	-0.19747	0.284131	88368.31	-88368.31	-132203.96

Table 2. The coefficients a_{ij} of the linearized system in the steady states

The values of the numbers a_{ij} in the considered cases are given in Table 2. It is easy to verify that in all cases the Hurwitz condition are satisfied.

In Fig. 10 simulations of the silicon tube growth is presented when the seed length is 10^{-2} and the radii of the seed are $R_i = 4.3389\times10^{-3}$ [m]; $R_e = 4.659\times10^{-3}$ [m]. The meniscus height at the start is $h = 2.14838\times10^{-4}$ [m].

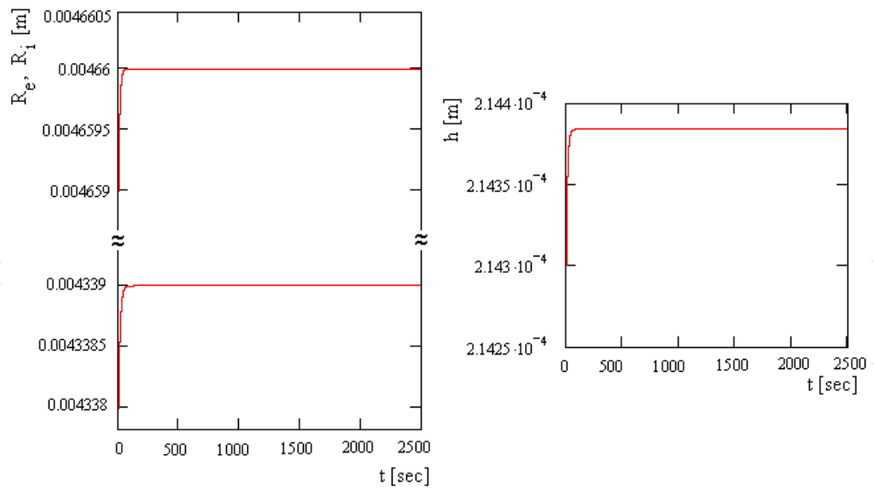

Fig. 10. The evolution of the outer radius, the inner radius of the tube and the meniscus height obtained integrating numerically the system (1) for $F_1 = 2 / R_e$, $\overline{v} = 1.6585917365 \cdot 10^{-4}$ [m/s], $T_0 = 1714.81$ [K] and $T_{en}(0) = 400[K]$

6. Conclusions

Knowing the material constants (density, heat conductivity, etc), the size of the single crystal tube which will be grown from that material, the size of the shaper which will be used and the cooling gas temperature at the entrance, it is possible to predict values of pulling rate, temperature at the meniscus basis, cooling gas temperature at the exit, vertical temperature gradient in the furnace, inner and outer walls cooling gas pressure differences, melt column height differences, crystallization front level, which can be used for a stable growth.

According to the model the predicted values are not unique i.e. there are several possibility to obtain a tube with prior given size from a given material using the same shaper. So, even if in our computation the material and the size of the shaper and tube is the same as in [Eriss] experiment, the computed data given in Table 1 can be different from that used in the real experiment. For this reason our purpose is not rely to compare the computed results with the experimental data. Moreover we want to reveal that a tube of prior given size can be obtained by different settings and the model permit to compute such settings. The choice of a specific setting is the practical crystal grower decision. The model provide possible settings and can be helpful in a new experiment planning.

Concerning the limits of the model it is clear that it is limited in applicability, as all models. The main limits are those introduced by approximations made in equations defining the model.

7. Appendix 1. Inequalities for single crystal tube growth by E.F.G. technique - Convex outer and inner free surface

Consider the differential equation (6) for $\frac{R_{gi} + R_{ge}}{2} \le r_e \le R_{ge}$, α_c, α_g such that $\alpha_g \in \left(0, \pi/2\right)$, $0 < \alpha_c < \pi/2 - \alpha_g$.

Definition 1. A solution $z = z(x)$ of the eq. (6) describes the outer free surface of a static meniscus on the interval $\left[r_e, R_{ge}\right]$ if it possesses the following properties: $z\left(R_{ge}\right) = 0$, $z'(r_e) = -\tan\left(\pi/2 - \alpha_g\right)$, $z'\left(R_{ge}\right) = -\tan\alpha_c$ and $z(r)$ is strictly decreasing on $[r_e, R_{ge}]$. The described outer free surface is convex on $[r_e, R_{ge}]$ if $z''(r) > 0 \quad \forall r \in [r_e, R_{ge}]$.

Theorem 1. If there exists a solution of the eq. (6), which describes a convex outer free surface of a static meniscus on the closed interval $[r_e, R_{ge}]$, then for $n = \frac{R_{ge}}{r_e}$, p_e satisfy:

$$-\gamma \cdot \frac{\pi/2 - \left(\alpha_c + \alpha_g\right)}{R_{ge}} \cdot \frac{n}{n-1} \cdot \cos\alpha_c + \frac{\gamma}{R_{ge}} \cdot \sin\alpha_c \le p_e$$
$$\le -\gamma \cdot \frac{\pi/2 - \left(\alpha_c + \alpha_g\right)}{R_{ge}} \cdot \frac{n}{n-1} \cdot \sin\alpha_g + \frac{\rho \cdot g \cdot R_{ge} \cdot (n-1)}{n} \cdot \tan\left(\pi/2 - \alpha_g\right) + \quad \text{(A.1.1)}$$
$$+ \frac{\gamma}{R_{ge}} \cdot n \cdot \cos\alpha_g$$

Theorem 2. Let be n such that $1 < n < \frac{2 \cdot R_{ge}}{R_{gi} + R_{ge}}$. If p_e satisfies the inequality:

$$p_e < -\gamma \cdot \frac{\pi/2 - \left(\alpha_c + \alpha_g\right)}{R_{ge}} \cdot \frac{n}{n-1} \cdot \cos\alpha_c + \frac{\gamma}{R_{ge}} \cdot \sin\alpha_c \quad \text{(A.1.2)}$$

then there exists $r_e \in \left[\frac{R_{ge}}{n}, R_{ge}\right]$ such that the solution of the initial value problem:

$$\begin{cases} z'' = \frac{\rho \cdot g \cdot z - p_e}{\gamma} \cdot \left[1 + (z')^2\right]^{3/2} - \frac{1}{r} \cdot \left[1 + (z')^2\right] \cdot z' \text{ for } \frac{R_{gi} + R_{ge}}{2} < r \le R_{ge} \\ z\left(R_{ge}\right) = 0,\ z'\left(R_{ge}\right) = -\tan\alpha_c \end{cases} \quad \text{(A.1.3)}$$

on the interval $[r_e, R_{ge}]$ describes the convex outer free surface of a static meniscus.

Corollary 3. If for p_e the following inequality holds:

$$p_e < -2 \cdot \gamma \cdot \frac{\pi/2 - (\alpha_c + \alpha_g)}{R_{ge} - R_{gi}} \cdot \cos\alpha_c + \frac{\gamma}{R_{ge}} \cdot \sin\alpha_c \quad \text{(A.1.4)}$$

then there exists $r_e \in \left(\frac{R_{ge} + R_{gi}}{2}, R_{ge}\right)$ (close to $\frac{R_{ge} + R_{gi}}{2}$) such that the solution of the i.v.p. (12) on the interval $[r_e, R_{ge}]$ describes a convex outer free surface of a static meniscus.

Corollary 4. If for $1 < n' < n < \dfrac{2 \cdot R_{ge}}{R_{gi} + R_{ge}}$ the following inequalities holds:

$$-\gamma \cdot \frac{\pi/2 - (\alpha_c + \alpha_g)}{R_{ge}} \cdot \frac{n'}{n'-1} \cdot \sin\alpha_g + \rho \cdot g \cdot R_{ge} \cdot \frac{n'-1}{n'} \cdot \tan\left(\pi/2 - \alpha_g\right) + \frac{\gamma}{R_{ge}} \cdot n' \cos\alpha_g$$
$$< p_e < -\gamma \cdot \frac{\pi/2 - (\alpha_c + \alpha_g)}{R_{ge}} \cdot \frac{n}{n-1} \cdot \cos\alpha_c + \frac{\gamma}{R_{ge}} \cdot \sin\alpha_c \tag{A.1.5}$$

then there exists $r_e \in \left[\dfrac{R_{ge}}{n}, \dfrac{R_{ge}}{n'}\right]$ such that the solution of the i.v.p. (A.1.3) on the interval $[r_e, R_{ge}]$ describes a convex outer free surface of a static meniscus.

Theorem 5. If a solution $z_1 = z_1(r)$ of the eq. (6) describes a convex outer free surface of a static meniscus on the interval $[r_e, R_{ge}]$, then it is a weak minimum for the energy functional of the melt column (7).

Definition 2. A solution $z = z(x)$ of the eq.(8) describes the inner free surface of a static meniscus on the interval $\left[R_{gi}, r_i\right]$, $\left(R_{gi} < r_i < \dfrac{R_{gi} + R_{ge}}{2}\right)$ if it possesses the following properties: $z'\left(R_{gi}\right) = \tan\alpha_c$, $z'(r_i) = \tan\left(\pi/2 - \alpha_g\right)$, $z\left(R_{gi}\right) = 0$ and $z(r)$ is strictly increasing on $[R_{gi}, r_i]$. The described inner free surface is convex on $[R_{gi}, r_i]$ if $z''(r) > 0$, $\forall r \in [\mathrm{R_{gi}}, r_i]$.

Theorem 6. If there exists a solution of the eq. (8), which describes a convex inner free surface of a static meniscus on the closed interval $[R_{gi}, r_i]$ and $r_i = m \cdot R_{gi}$ with $1 < m < \dfrac{R_{gi} + R_{ge}}{2 \cdot R_{gi}}$, then the following inequalities hold:

$$-\gamma \cdot \frac{\pi/2 - \left(\alpha_c + \alpha_g\right)}{(m-1) \cdot R_{gi}} \cdot \cos\alpha_c - \frac{\gamma}{R_{gi}} \cdot \cos\alpha_g \le p_i$$
$$\le -\gamma \cdot \frac{\pi/2 - \left(\alpha_c + \alpha_g\right)}{(m-1) \cdot R_{gi}} \cdot \sin\alpha_g + \rho \cdot g \cdot R_{gi} \cdot (m-1) \cdot \tan\left(\pi/2 - \alpha_g\right) - \frac{\gamma}{m \cdot R_{gi}} \cdot \sin\alpha_c \tag{A.1.6}$$

Theorem 7. Let m be such that $1 < m < \dfrac{R_{gi} + R_{ge}}{2 \cdot R_{gi}}$. If p_i satisfies the inequality:

$$p_i < -\gamma \cdot \frac{\pi/2 - \left(\alpha_c + \alpha_g\right)}{(m-1) \cdot R_{gi}} \cdot \cos\alpha_c + \frac{\gamma}{R_{gi}} \cdot \cos\alpha_g \tag{A.1.7}$$

then there exists $r_i \in [R_{gi}, m \cdot R_{gi}]$, such that the solution of the initial value problem:

$$\begin{cases} z'' = \dfrac{\rho \cdot g \cdot z - p_i}{\gamma} \cdot \left[1 + (z')^2\right]^{3/2} - \dfrac{1}{r} \cdot \left[1 + (z')^2\right] \cdot z' \text{ for } R_{gi} < r \le \dfrac{R_{gi} + R_{ge}}{2} \\ z(R_{gi}) = 0, \; z'(R_{gi}) = \tan \alpha_c \end{cases} \quad \text{(A.1.8)}$$

on the interval $[R_{gi}, r_i]$ describes the convex inner free surface of a static meniscus.

Corollary 8. If for p_i the following inequality holds,

$$p_i < -2 \cdot \gamma \cdot \frac{\pi/2 - (\alpha_c + \alpha_g)}{R_{ge} - R_{gi}} \cdot \cos \alpha_c - \frac{\gamma}{R_{gi}} \cdot \cos \alpha_g \quad \text{(A.1.9)}$$

then there exists $r_i \in \left(R_{gi}, \dfrac{R_{gi} + R_{ge}}{2}\right)$ (close to $\dfrac{R_{gi} + R_{ge}}{2}$) such that the solution of the i.v.p. (A.1.8) on the interval $[R_{gi}, r_i]$ describes a convex inner free surface of a static meniscus.

Corollary 9. If for $1 < m' < m < \dfrac{R_{gi} + R_{ge}}{2 \cdot R_{gi}}$ the following inequalities hold

$$-\gamma \cdot \frac{\pi/2 - (\alpha_c + \alpha_g)}{(m' - 1) \cdot R_{gi}} \cdot \sin \alpha_g + \rho \cdot g \cdot R_{gi} \cdot (m' - 1) \cdot \tan\left(\pi/2 - \alpha_g\right) - \frac{\gamma}{m' \cdot R_{gi}} \cdot \sin \alpha_c \quad \text{(A.1.10)}$$

$$< p_i < -\gamma \cdot \frac{\pi/2 - (\alpha_c + \alpha_g)}{(m - 1) \cdot R_{gi}} \cdot \cos \alpha_c - \frac{\gamma}{R_{gi}} \cdot \cos \alpha_g$$

then there exists r_i in the interval $[m' \cdot R_{gi}, m \cdot R_{gi}]$ such that the solution of the i.v.p. (A.1.8) on the interval $[R_{gi}, r_i]$ describes a convex inner free surface of a static meniscus.

Theorem 10. If a solution $z_1 = z_1(r)$ of the eq. (8) describes a convex inner free surface of a static meniscus on the interval $[R_{gi}, r_i]$, then it is a weak minimum for the energy functional of the melt column (9).

8. Appendix 2. Inequalities for single crystal tube growth by E.F.G. technique - Concave outer and inner free surface

Consider the equation (6) for $0 < R_{gi} < \dfrac{R_{gi} + R_{ge}}{2} \le r_e < R_{ge}$, α_c, α_g such that $\alpha_g \in \left(0, \pi/2\right)$, $0 < \pi/2 - \alpha_g < \alpha_c < \pi/2$.

Definition 3. The outer free surface is concave on $[r_e, R_{ge}]$ if $z''(r) < 0$, $\forall r \in [r_e, R_{ge}]$.

Theorem 11. If there exists a concave solution $z_e = z_e(r)$ of the equation (6) then $n = \frac{R_{ge}}{r_e}$ and p_e satisfy the following inequalities:

$$\frac{n}{n-1}\cdot\gamma\cdot\frac{\alpha_c+\alpha_g-\pi/2}{R_{ge}}\cdot\cos\alpha_c+\frac{\gamma}{R_{ge}}\cdot\cos\alpha_g \le p_e \le \frac{n}{n-1}\cdot\gamma\cdot\frac{\alpha_c+\alpha_g-\pi/2}{R_{ge}}\cdot\sin\alpha_g + \frac{n-1}{n}\cdot\rho\cdot g\cdot\tan\alpha_c+\frac{n\cdot\gamma}{R_{ge}}\cdot\sin\alpha_c \tag{A.2.1}$$

Theorem 12. If for $1 < n' < n < \frac{2\cdot R_{ge}}{R_{ge}+R_{gi}}$ and p_e the inequalities hold:

$$\frac{n}{n-1}\cdot\gamma\cdot\frac{\alpha_c+\alpha_g-\pi/2}{R_{ge}}\cdot\sin\alpha_g+\frac{n-1}{n}\cdot\rho\cdot g\cdot R_{ge}\cdot\tan\alpha_c+\frac{n\cdot\gamma}{R_{ge}}\cdot\sin\alpha_c < p_e < \frac{n'}{n'-1}\cdot\gamma\cdot\frac{\alpha_c+\alpha_g-\pi/2}{R_{ge}}\cdot\cos\alpha_c+\frac{\gamma}{R_{ge}}\cdot\cos\alpha_g. \tag{A.2.2}$$

then there exists $r_e \in \left[\frac{R_{ge}}{n}, \frac{R_{ge}}{n'}\right]$ and a concave solution of the equation (6).

Theorem 13. A concave solution $z_e(r)$ of the equation (6) is a weak minimum of the free energy functional of the melt column (7).

Consider now the differential equation (8) for $0 < R_{gi} < r_i < \frac{R_{gi}+R_{ge}}{2} < R_{ge}$ and α_c, α_g such that $0 < \pi/2 - \alpha_g < \alpha_c < \pi/2$, $\alpha_g \in \left(0, \pi/2\right)$.

Theorem 14. If there exists a concave solution $z_i = z_i(r)$ of the equation (8) then $m = \frac{r_i}{R_{gi}}$ and p_i satisfies the following inequalities:

$$\frac{1}{m-1}\cdot\gamma\cdot\frac{\alpha_c+\alpha_g-\pi/2}{R_{gi}}\cdot\cos\alpha_c-\frac{\gamma}{R_{gi}}\cdot\sin\alpha_c \le p_i \le \frac{1}{m-1}\cdot\gamma\cdot\frac{\alpha_c+\alpha_g-\pi/2}{R_{gi}}\cdot\sin\alpha_g + (m-1)\cdot\rho\cdot g\cdot R_{gi}\cdot\tan\alpha_c-\frac{\gamma}{m\cdot R_{gi}}\cdot\cos\alpha_g \tag{A.2.3}$$

Theorem 15. If for $1 < m' < m < \frac{2\cdot R_{ge}}{R_{ge}+R_{gi}}$ and for p_i the following inequalities hold:

$$\frac{1}{m-1}\cdot\gamma\cdot\frac{\alpha_c+\alpha_g-\pi/2}{R_{ge}}\cdot\sin\alpha_g+(m-1)\cdot\rho\cdot g\cdot R_{gi}\tan\alpha_c-$$
$$\frac{\gamma}{m\cdot R_{gi}}\cdot\cos\alpha_g<p_i<\frac{1}{m'-1}\cdot\gamma\cdot\frac{\alpha_c+\alpha_g-\pi/2}{R_{gi}}\cdot\cos\alpha_c+\frac{\gamma}{R_{gi}}\cdot\sin\alpha_c \tag{A.2.4}$$

then there exists r_i in the interval $\left[m'\cdot R_{gi}, m\cdot R_{gi}\right]$ and a concave solution of the eq. (8).

Theorem 16. A concave solution $z_i(r)$ of the equation (8) is a weak minimum of the free energy functional of the melt column (9).

9. References

St. Balint, A.M. Balint (2009), *On the creation of the stable drop-like static meniscus, appropriate for the growth of a single crystal tube with prior specified inner and outer radii*, Mathematical Problems in Engineering, vol. 2009, Article ID:348538 (2009), pp 1-22

St. Balint, A.M. Balint (2009), *Inequalities for single crystal tube growth by edge-defined film-fed (E.F.G.) technique* , Journal of Inequalities and Applications, vol.2009, Article ID: 732106, pp.1-28

St.Balint, A.M.Balint, L.Tanasie (2008) - *The effect of the pressure on the static meniscus shape in the case of tube growth by edge-defined film-fed growth (E.F.G.) method*, Journal of Crystal Growth, Vol. 310, pp.382-390

St. Balint, L.Tanasie (2008), *Nonlinear boundary value problems for second order differential* equations describing concave equilibrium capillary surfaces, Nonlinear Studies 15, Vol. 4, pp.277-296.

St.Balint, L.Tanasie(2011), *Some problems concerning the evaluation of the shape and size of the meniscus occurring in silicon tube growth* - Mathematics in Engineering, Science and Aerospace Vol. 2, pp. 53-70.

St.Balint, L.Tanasie (2010), *A procedure for the determination of the angles* $\tilde{\alpha}_e^0(r_e,h_e;p_e)$ *and* $\tilde{\alpha}_i^0(r_i,h_i;p_i)$ *which appears in the nonlinear system of differential equations describing the dynamics of the outer and inner radius of a tube, grown by the edge-defined film-fed growth (EFG) technique*, Nonlinear Analysis: Real World Applications, Vol. 11(Issue 5), pp 4043-4053

St.Balint, L.Tanasie (2011), *The choice of the pressure of the gas flow and the melt level in silicon tube growth,* Mathematics in Engineering, Science and Aerospace, Vol. 4, pp.

H.Behnken, A.Seidl and D.Franke (2005), *A 3 D dynamic stress model for the growth of hollow silicon polygons*, Journal of .Crystal Growth, Vol 275, pp. e375-e380.

A.V.Borodin, V.A.Borodin, V.V.Sidorov and I.S.Petkov (1999), *Influence of growth process parameters on weight sensor readings in the Stepanov (EFG) technique*, Journal of .Crystal Growth, Vol. 198/199, pp.215-219.

A.V.Borodin, V.A.Borodin and A.V.Zhdanov (1999), *Simulation of the pressure distribution in the melt for sapphire ribbon growth by the Stepanov (EFG) technique*, Journal of .Crystal Growth, Vol. 198/199, pp.220-226.

L.Erris, R.W.Stormont, T.Surek, A.S.Taylor (1980), *The growth of silicon tubes by the EFG process*, Journal of .Crystal Growth, Vol. 50, pp.200-211.

R. Finn, *Equilibrium capillary surfaces* (1986), Vol. 284, Grundlehren der mathematischen Wissenschaften, Springer, New York, NY, USA.

I.P.Kalejs, A.A.Menna, R.W.Stormont and I.W.Hudrinson (1990), *Stress in thin hollow silicon cylinders grown by the edge-defined film-fed growth technique*, Journal of .Crystal Growth, Vol 104, pp.14-19.

H.Kasjanow, A.Nikanorov, B.Nacke, H.Behnken, D.Franke and A.Seidl (2007), 3Dcoupled electromagnetic and thermal modeling of EFG silicon tube growth, Journal of .Crystal Growth, Vol. 303, pp.175-179.

B.Mackintosh, A.Seidl, M.Quellette, B.Bathey, D.Yates and J.Kalejs (2006) *Large silicon crystal hollow-tube growth by the edge-defined film-fed growth (EFG) method*, Journal of .Crystal Growth, Vol 287, pp.428-432.

S.Rajendram, M.Larousse, B.R. Bathey and J.P.Kalejs (1993), *Silicon carbide control in the EFG system*, Journal of .Crystal Growth, Vol. 128, pp.338-342.

S.Rajendram, K.Holmes and A.Menna (1994), *Three-dimensional magnetic induction model of an octagonal edge-defined film-fed growth system*, Journal of .Crystal Growth, Vol. 137(No 1-2), pp.77-81.

S.N.Rossolenko (2001), *Menisci masses and weights in Stepanov (EFG) technique: ribbon, rod, tube*, Journal of .Crystal Growth, vol. 231, pp.306-315.

A.Roy, B.Mackintosh, J.P.Kalejs, Q.S.Chen, H.Zhang and V.Prasad(2000), *A numerical model for inductively heated cylindrical silicon tube growth system*, Journal of Crystal Growth , Vol 211, pp.365-371.

A.Roy, H.Zhang, V.Prasad, B.Mackintosh, M.Quellette and J.Kalejs (2000), *Growth of large diameter silicon tube by EFG technique: modeling and experiment*, Journal of .Crystal Growth , Vol 230, pp.224-231.

D.Sun, Ch.Wang, H.Zhang, B.Mackintosh, D.Yates and J.Kalejs (2004), *A multi-block method and multi-grid technique for large diameter EFG silicon tube growth*, Journal of .Crystal Growth, Vol 266, pp. 167-174

T.Surek, B.Chalmers and A.I.Mlavsky (1977), *The edge film-fed growth of controlled shape crystals*, Journal of .Crystal Growth, Vol. 42, pp.453-457

J.C.Swartz, T.Surek and B.Chalmers (1975), *The EFG process applied to the growth of silicon ribbons*, J.Electron.Mater, Vol. 4, pp.255-279.

L.Tanasie, St.Balint (2010) , *Model based, pulling rate, thermal and capillary conditions setting for silicon tube growth*, Journal of Crystal Growth, vol. 312, pp. 3549-3554

V.A.Tatarchenko (1993), *Shaped crystal growth*, Kluwer Academic Publishers, Dordrecht.

B.Yang, L.L.Zheng, B.MacKintosh, D.Yates and J.Kalejs (2006), *Meniscus dynamics and melt solidification in the EFG silicon tube growth process,* Journal of .Crystal Growth, Vol. 293, pp.509-516.

© 2012 The Author(s). Licensee IntechOpen. This is an open access article distributed under the terms of the Creative Commons Attribution 3.0 License, which permits unrestricted use, distribution, and reproduction in any medium, provided the original work is properly cited.

IntechOpen

IntechOpen